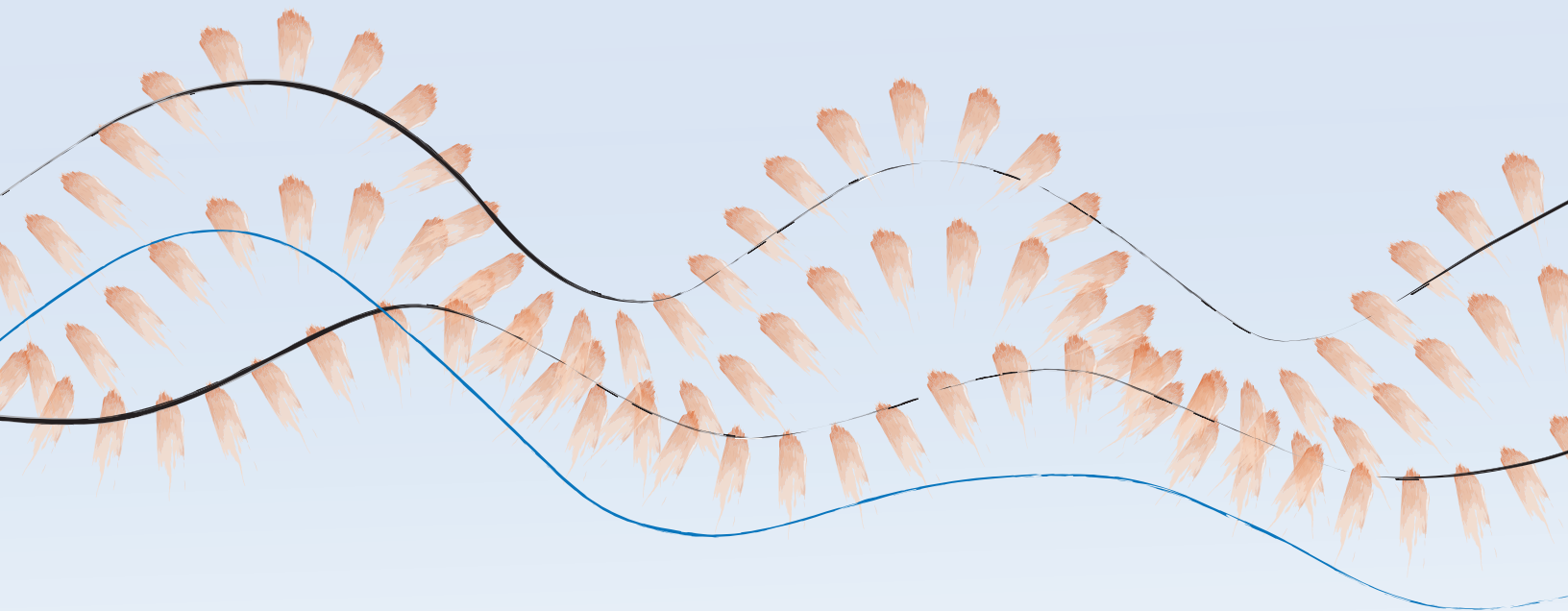# Soft Robot Locomotion
with
Metachronal Waves

Janne Willems van Dijk

Soft Robot Locomotion with Metachronal Waves

by

Janne Willems van Dijk

to obtain the degree of Master of Science
at the Delft University of Technology,
to be defended on November 9th 2022.

CONTENTS

Soft Robot Locomotion with Metachronal Waves

Janne Willems van Dijk

Abstract—**Conventional robots adopt wheels or robotic limbs for locomotion. Wheels are simple to control but not suitable for irregular terrains. On the other hand, robotic feet can overcome a wider variety of surfaces but are less desirable due to their complex design and control system. In nature, we find that invertebrate animals, like snails, can go anywhere without needing the complex control system a rigid robot needs. Instead, they move forward by sending travelling deformations along their soft bodies. Inspired by these animals, we present a soft robot that uses a sequence of deformations for locomotion. This sequence of deformations is driven by a row of vibrating actuators that vibrate with the same frequency but a phase shift between each consecutive actuator. The metachronal wave arising from this vibration pattern offers efficient locomotion due to the continuous movement of the robot. The top speed achieved in this research was $5\ mm/s$ for both forward and backward locomotion. Our study shows how the robot's locomotion capabilities are affected by its material and how the robot's velocity depends on the mechanical design and the properties of the metachronal wave and provides a next step into soft robots that can efficiently move almost anywhere.**

I. INTRODUCTION

What if we need to get access to areas affected by a natural disaster, buildings that are at the point of falling down, or places that are so deep or small that we cannot reach them ourselves? We use robots. This robot might use wheels to move, which limits its locomotion range to flat surfaces. It might use feet, which does open up a lot more possibilities, but is very expensive to achieve and complex to control. An inexpensive solution could be to make the robot soft, since the soft material already provides a safe interaction and adaptability with the environment.

Soft robots are robots with soft or compliant parts embedded into their mechanical structure. These materials give soft robots the ability to shape and conform around objects they encounter. This ability makes a soft robot a lot safer in human robot interaction compared to rigid robotics and useful for moving around in complex and fragile environments [1].

The soft structure of most soft robots allows deformations with infinite degrees of freedom, which opens up possibilities for new actuation principles that cannot be employed by rigid robots. In addition to the new actuation principles, the soft structure also allows different locomotion patterns. Soft robots can not only walk and roll, they can also slither, crawl, jump, and swim [2].

A lot of these locomotion patterns are inspired by invertebrate animals, like centipedes, earthworms and snails. These animals can come almost anywhere, through wet, dry, loose, and inclined surfaces and through spaces most people or robots cannot go. A lot of invertebrate animals use traveling deformations, or waves, along their body for locomotion. This continuous motion allows them to not get stuck, like limbs and wheels may do, while keeping agility in complex environments. Continuous traveling deformations is also an efficient way of locomotion, since all energy that is put into the deformation is used for forward motion, in contrast to for example jumping, where part of the energy is pointed backwards.

The traveling deformation in a soft body is caused by the actuation of separate parts in a sequence. Such a wave is also called a metachronal wave, since it is not caused by one motion that travels through a material, but by the sequence of individual motions with a phase shift.

Soft robots already exist that use metachronal waves for their locomotion. Some use pneumatic actuation [3]–[6], the most common type of actuation found in soft robotics. Pneumatic actuation is very versatile, and can have very high power, while the robot itself remains completely soft. However, this versatility and high power is only achieved when the robot is tethered to a large compression source. When this compression source is condensed to small parts that are incorporated into the robot, it loses a lot of the power, and the robot is not completely soft anymore. Other soft robots move by inducing metachronal waves with a rotating magnetic field [7], [8]. These robots are made out of a soft silicone with magnetic particles inside. The magnetic particles are orientated in a way, that when a magnetic field is applied, each particle reacts slightly different, and the robot can be curved in the shape of a sine wave, or any other desired curvature. This means, that each magnetic particle represents a slightly different phase of the sine wave. When the magnetic field starts rotating, each magnetic particle will rotate with it, and the body will deform like a traveling wave and move forward.

What all these soft robots have in common, is that they all have a small range of motion. The pneumatic robots are tethered to a pressure source, which limits the range they can travel to the length of the tether. When this pneumatic robot becomes untethered and carries the necessary equipment with it, its velocity drastically decreases. The magnetic robots only work inside rotating magnetic fields, which is also a highly controlled environment in a limited space.

A soft robot that can move freely using traveling deformations needs a different actuation principle. Therefore, in this research is the metachronal wave generated by a sequence of vibrations with a phase shift. Vibrating actuators are often small and require very little power. By encapsulating these vibrating actuators inside a soft body, the robot can move without any limiting rigid components outside.

The goal of this research is to make a soft robot move with a metachronal wave generated by a sequence of vibrations with a phase shift. By switching the phase shift from positive to negative, the direction of locomotion can be inverted. The model described in the next section shows how the parameters of

both the vibration and robot design influence the metachronal wave and how this wave can lead to locomotion. Furthermore, the influence of the wave parameters on the propagation of the metachronal wave and the locomotion of the robot is tested and analysed for robots made from different soft materials.

II. METACHRONAL WAVE LOCOMOTION MODEL

The robot is a rectangular soft beam with, along the centre line, a row of vibrating actuators with equal spacing in between, see Figure 1. The actuators all vibrate with the same frequency f and fixed phase shift φ between each consecutive actuator. This imposes a metachronal wave along the beam.

A. From Vibrations to Metachronal Wave

The metachronal wave along the beam mimics a transverse traveling wave, where the deformation is perpendicular to the direction the wave travels in. A transverse traveling wave origins from a vibration applied to a medium, which then propagates through this medium. In a way, along this medium there is an infinite number of vibrating points that all vibrate with the same frequency, but a slightly shifted phase shift between each consecutive point. The metachronal wave along the robot is similar, but now a finite number of points with more space in between are individually actuated to vibrate with transverse displacement v_n:

$$v_n(t) = a\sin(\omega t + \varphi_n) \tag{1}$$

In this formula, the phase shift between each actuator is $\varphi_n = [0, \varphi, 2\varphi, ..., (N-1)\varphi]$. As said before, the metachronal wave mimics a transverse traveling wave, which in its simplest form follows the formula:

$$v(x,t) = a\sin(\frac{2\pi}{\lambda}x + \omega t) \tag{2}$$

Here, the amplitude of the vibration is a, the wavelength λ and the rotational frequency is $\omega = 2\pi f$. In this example there are $N = 6$ actuators, with an equal distance δ between each one, on top of the robot. When the curvature of the centre line is exactly one wavelength of the sine wave, the expected curvature would look like the line in Figure 1. On this line the actuators are spaced equally and thus the phase shift between each actuator can be calculated.

Since the distance between the actuators is constant, the x coordinate of each actuator is $x_n = [0, \delta, 2\delta, ..., (N-1)\delta]$. At these points, Equation 1 and Equation 2 are the same, and $\varphi_n = \frac{2\pi}{\lambda}x_n$. Solving this equation for the wavelength gives:

$$\lambda = \frac{2\pi\delta}{\varphi} \tag{3}$$

Implementation of Equation 3 into Equation 2, gives a formula for the metachronal wave described in parameters that can be adjusted in the setup, being φ, δ and ω:

$$v(x,t) = a\sin(\frac{\varphi}{\delta}x + \omega t) \tag{4}$$

The wave speed of the metachronal wave is then:
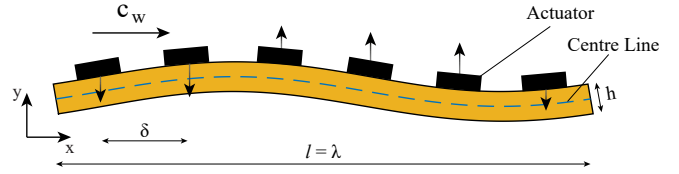
$$c_w = \frac{\omega\delta}{\varphi} \tag{5}$$

Fig. 1. **Side view of the proposed robot** with 6 actuators spaced out with distance δ in between with a thickness h and length l. The centre line (blue dashed line) of the robot follows one wavelength λ of a transverse wave traveling to the right, where the arrows point in the direction the actuator will move to next.
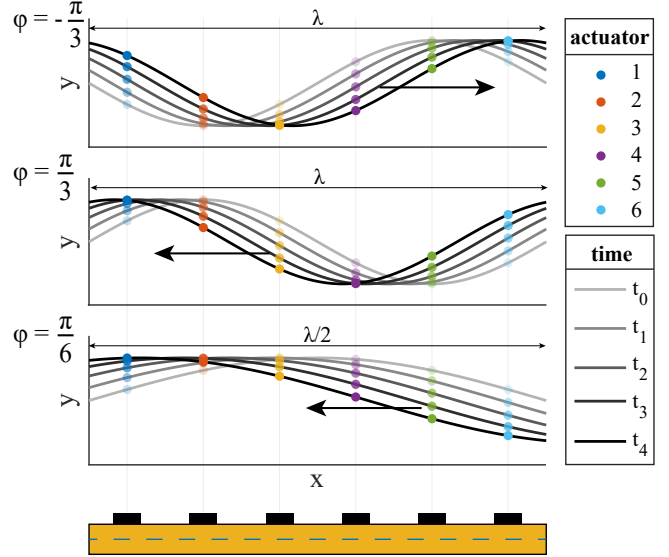

Fig. 2. **The influence of the phase shift on the wavelength along the robot** with 6 actuators at a fixed distance. The amplitude in y direction is exaggerated compared to real life, since the real amplitude is only $20-150\ \mu m$. In the top graph the robot follows the curvature of one wavelength λ of the metachronal wave with a phase shift of $\varphi = -\pi/3$. In the centre graph the direction of the wave changes for a positive phase shift $\varphi = \pi/3$, but the wavelength remains the same. In the bottom graph the phase shift is divided by two to $\varphi = \pi/6$, which increases the wavelength by two, while only half of that wavelength is sampled along the robot.

With these formulas we know how to adjust the phase shift φ and actuator spacing δ to get a certain metachronal wave in the robot. For example, following Equation 3, the wavelength can be increased both by increasing the spacing δ and decreasing the phase shift φ. The effect of changing the phase shift is further elaborated in Figure 2. Overall, the values for δ and φ together define the spatial sampling of the traveling sine wave. The spacing δ changes the length of the robot. When the spacing is increased but the phase shift remains the same, the wavelength will increase with the spacing and the number of points that vibrate and contribute to one wavelength of the metachronal wave remains the same. On the other hand, when the spacing remains the same but the phase shift is increased, the wavelength will be decreased. This decrease in wavelength means that more cycles of the wave are present inside the robot while still only 6 points are being vibrated. This means that less points contribute to one wavelength and the sampling of the wave is changed.
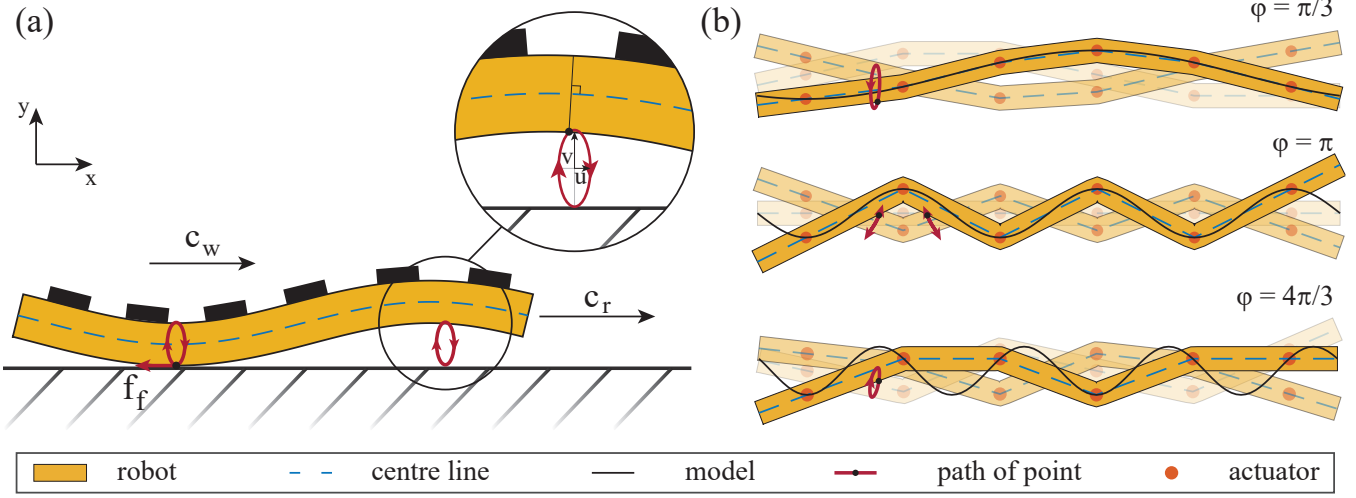
Fig. 3. Illustration of the metachronal wave locomotion model and the influence of sampling. (a) The centre line of the robot (blue dashed line) curves like one wavelength of a metachronal wave, due to a phase shift of $\varphi = \pi/3$. Since the robot is assumed to be an Euler-Bernoulli beam, the points on the bottom of the robot always stay perpendicular to the centre line curvature, with transverse displacement v and longitudinal displacement u. With the centre line curvature following the metachronal wave, the points on the bottom of the robot will follow an ellipsoidal motion, visualized in red. When a point touches the ground, a force f_f will push the robot forward with a certain velocity c_r. (b) To illustrate the effect of the sampling on the wave, the sampled points that vibrate are connected by straight centre lines and the robot is build around it following Euler-Bernoulli theory. The top illustration shows the robot with $\varphi = \pi/3$ and 6 points are sampled in one wavelength. The robot follows the modeled centre line accurately. The centre illustration shows the robot when consecutive actuators vibrate out of phase with $\varphi = \pi$. In this case the points will only move up and down and a standing wave appears along the robot, preventing locomotion. The bottom illustration shows that when the phase shift is further increased to $\varphi = 4\pi/3$, aliasing appears and the robot will follow a wave with that is equal to the wave that appears with a phase shift of $\varphi = -2\pi/3$, which has a larger wavelength and travels in the opposite direction.

B. Metachronal Wave to Locomotion

The soft robot is assumed to be an Euler-Bernoulli beam, since the deflection of the beam as a result of the vibrations is small compared to the size of the beam: the vibration amplitude is between $20-100$ micron, while the beam itself is between $70-150\ mm$ long. The beam is only subjected to lateral loads and stays in the linear elasticity range, which means that the Euler-Bernoulli theory holds and the shear deformation and rotary inertia effects can be neglected.

The lateral load on the beam is caused by the vibrations on the beam and induces a transverse displacement v along the centre line of the beam that follows the metachronal wave described by Equation 4. According to Euler-Bernoulli theory, all points on the bottom and top of the beam stay perpendicular to the centre line of the beam, as depicted in Figure 3a. To calculate the trajectory of these points, first the longitudinal displacement u needs to be calculated [9]:

$$u(x, y, t) = -y\frac{\partial v}{\partial x} = -ayk\cos(\omega t + kx) \qquad (6)$$

Where $y = h/2$ is the distance from the centre line and the wave number $k = \varphi/\delta$. Each point on the bottom surface then follows the shape of an ellipse with the formula:

$$\frac{u^2}{(ayk)^2} + \frac{v^2}{a^2} = 1 \qquad (7)$$

Since each bottom point follows an ellipsoidal motion, the robot's body doesn't only move up and down with the vibrations, but also sideways. Due to this sideways motion, the robot can move forward and backward, depending on the direction of the metachronal wave and the frictional coefficient between the robot surface and the ground [10].

When the curvature of the robot follows a standing wave the robot will not move forward, since the points on the bottom only follow half the ellipsoid up and down.

C. Sampling

The ellipsoidal motion of the robot will only appear when the metachronal wave along the robot imitates the desired transverse traveling wave from Equation 4. Hence, enough points in one wavelength need to be sampled to avoid aliasing effects. As determined before, the sampling of the wave depends on the phase shift φ. In Figure 3b the effect of the sampling is further illustrated: when the sampled points, or the actuators, vibrate with a phase shift smaller than π, the robot will generate a metachronal wave that follows the model. When the phase shift is equal to π, the actuators will vibrate out of phase and generate a standing wave, which will only make the robot go up and down, instead of moving forward or backward. When the phase shift is larger than π, a metachronal wave with a larger wavelength and opposite direction to the model will appear. Thus the model only holds for input sequences with a phase shift φ between $-\pi$ and π.

D. Robot Velocity Estimation

To further design the robot, we need to know how the parameters of the robot and metachronal wave affect the performance of the robot. For this, we estimated the velocity of the robot itself. This robot velocity c_r is equal in value and opposite in sign to the instantaneous velocity at a point p on

the bottom of the robot that is in contact with the ground [11], this velocity can be written as:

$$c_r(t) = -\dot{x}_p(t) = -\frac{\partial u}{\partial t} = a\frac{h}{2}k\omega\sin(\omega t + kx_c) \quad (8)$$

At the point that touches the bottom, the derivative is zero [5], which gives:

$$\frac{\partial v}{\partial x_p} = ak\cos(\omega t + kx_p) = 0, \quad x_p = \frac{1}{k}\tan^{-1}(\frac{\cos(\omega t)}{\sin(\omega t)}) \quad (9)$$

Implementing Equation 9 into Equation 8, gives the following formula for the velocity:

$$c_r(t) = a\frac{h}{2}k\omega\sin(\omega t + \tan^{-1}(\frac{\cos(\omega t)}{\sin(\omega t)})) \quad (10)$$

The estimation for the average velocity of the robot can be found by taking the integral over time of Equation 10, which after derivation is:

$$\bar{c}_r = \frac{1}{T}\int_0^T c_r(t)dt = a\frac{h}{2}k\omega = a\frac{h}{2}\frac{\varphi}{\delta}\omega \quad (11)$$

A more elaborate derivation of all the formulas used to calculate the average velocity of the robot can be found in Appendix A.

For a robot that has vibration amplitude $a = 30\ \mu m$, spacing $\delta = 12\ mm$, frequency $f = 250\ Hz$, the relationship between the wavelength and robot speed for various robot thicknesses h is visualized in Figure 4. The velocity drops significantly with increasing wavelength and eventually will go to zero. When one wavelength of the wave is present inside the robot for $\lambda = 72\ mm$ this robot is estimated to go $25\ mm/s$.
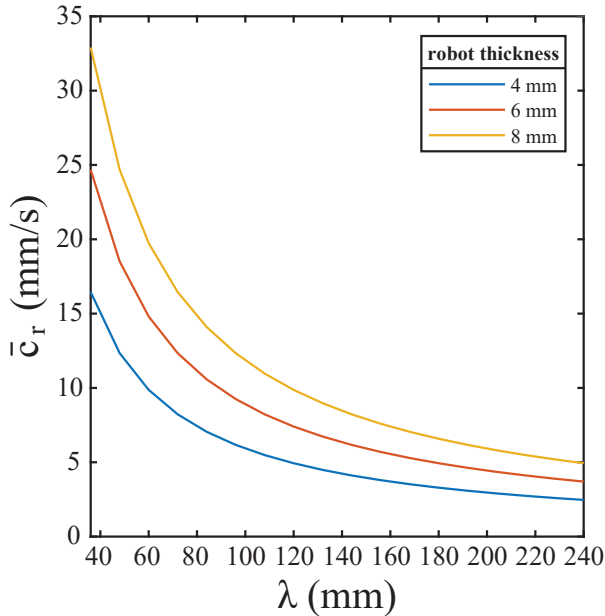

Fig. 4. **The relation between the estimated robot velocity and the metachronal wave.** The estimated average robot velocity of the metachronal wave locomotion model decreases with increasing wavelength λ. For increasing robot thickness h the estimated velocity also increases.

III. DESIGN

A. Actuation

For actuating the soft robot two components need to be chosen: the vibration source and the signal generation source. The vibration source needs to have a single-plane vibration, that is driven by an AC signal to make it easy to impose a phase shift. The actuator also needs to be small, in order to not restrict the bending abilities of the soft robot. The actuator chosen for this research is a linear resonant actuator (LRA). These actuators fulfill all the requirements stated above. A LRA is a small coin vibrator with a voice coil and a magnetic mass in the middle connected to a spring, as can be seen in Figure 5. By sending an AC signal through the voice coil, a magnetic field is generated, which makes the magnetic mass in the middle move up and down with the spring. Due to this spring being there, these actuators have a resonance effect, so work best at their natural resonant frequency, which is around $175 - 235\ Hz$ [12].

The actuators used in this research are model C08-005 from Precision Microdrives. This a LRA with resonant frequency $235\ Hz$ and RMS (root mean square) amplitude $1.8\ V$. They have a diameter of $8\ mm$ and are $3.3\ mm$ thick.
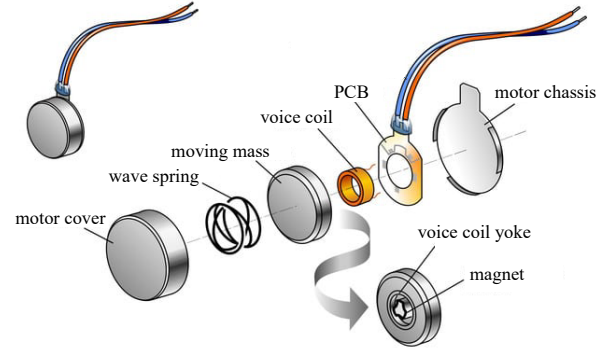
Fig. 5. **Exploded view of a linear resonant actuator.** Within the motor cover and chassis the moving mass attached to a wave spring, with a magnet and voice coil yoke inside the moving mass. The rest of the voice coil is inside attached to the PCB. The voice coil will generate a magnetic field which makes the mass move. Retrieved from [12].

Fig. 6. **The setup for signal generation.** In MATLAB the signals (v_n) are formulated and communicated to a DAQ board where the signals are generated. These signals are then amplified by three audio amplifiers (AudioAmp) and send to the actuators.

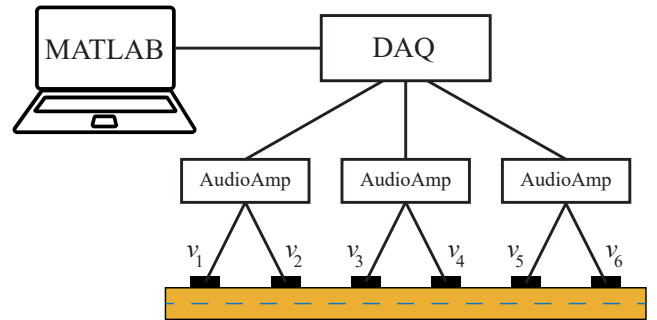The robots in this research use 6 actuators, therefore, 6 sine wave signals with different phase shifts need to be generated. In order to achieve this, a data acquisition system (DAQ) is used for generating the signals, specifically, the cDAQ-9174 CompactDAQ Chassis, with a NI-9264 C Series Voltage Output Module and a NI-9205 C Series Voltage Input Module. The Output Module is used for the generation of the 12 signals, the input module can later be used to synchronously gather data from external sources on the same time axis as the output signal, as will be described in section IV.

Since the DAQ cannot send high ampere signals, the signals need to be amplified. The amplifiers used in this research are the AudioAmp 2Click (MIKROE 3077). These are type D audio amplifiers that can amplify two signals at the same time. Each amplifier is powered by a breadboard power supply (HW 131). The full setup for the signal generation of the robot is visualized in Figure 6.

B. Robot

The initial robot was made from silicone (Ecoflex 0050, Smooth-On). This material was chosen, because it is flexible and easy to mold into a rectangular shape with the actuators embedded inside. The robot can be seen in Figure 7a. This rectangular beam robot has dimensions $l \times w \times h = 72 \times 14 \times 8\,mm$. Ecoflex is very flexible and also slightly sticky, so adhered strongly to the ground surface. Unfortunately, the vibration of the actuators did not have a big enough amplitude to generate a force large enough for this robot to move. Therefore, other soft materials were also investigated.

The second robots were made from rubber and one can be seen in Figure 7b. These robots were made from a $3\,mm$ black rubber sheet (506-3157, RS PRO). This rubber was already available in the lab, fulfilled the softness requirement and does not have the same stickiness property as the silicone did. However, the rubber sheet can be cut to size, but cannot be molded into any other shape and the thickness of the robot can only be a multiplication of the thickness of the sheet. To make the rubber robot, the sheet was first cut to size, then the actuators were stuck on top using double sided tape (Tesa fix 64621 and 3M 9087). One rubber robot with dimensions $l \times w \times h = 72 \times 14 \times 3\,mm$ was analysed.

The third and final material used for a robot was TPU 95A (Ultimaker), a flexible rubber-like 3D printer material made from thermoplastic polyurethane. This makes the body of the robot easy and fast to manufacture with a 3D printer. Since the robot can now be 3D printed, the rectangular beam design could be further expanded to a design with little feet on the bottom. These feet stretch along the width of the robot and provided some extra thickness to the robot, without blocking the ability of the body to curve like a sine wave. This extra thickness should make the soft robot faster compared to the rubber robot according to Equation 11. The robot has dimensions $l \times w \times h = 72 \times 14 \times 8\,mm$, see Figure 7c. It consists of 2 layers, the bottom layer has the 34 feet which are $1\,mm$ thick and the top layer is a $1\,mm$ sheet with holes to align the 6 actuators. Everything is connected with the same double sided tape as before.
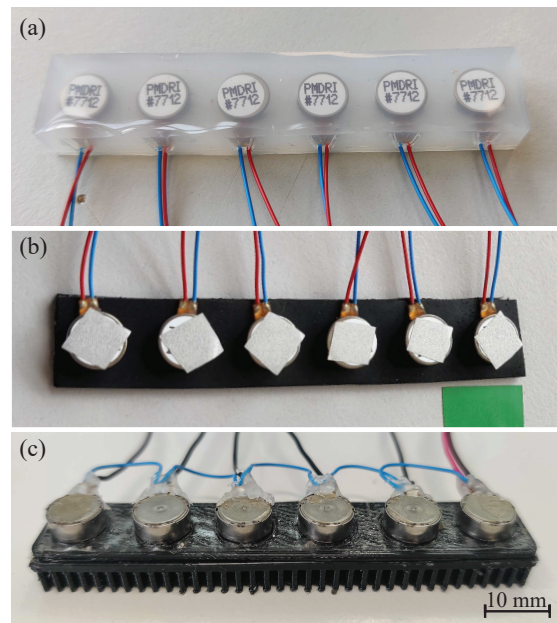

Fig. 7. **The robots used in this research**, all with 6 actuators, spacing $\delta = 12\,mm$ and length $l = 72\,mm$. (a) Silicone robot. (b) Robot with rubber sheet bottom. (c) TPU robot.

IV. EXPERIMENTAL METHOD

There are two types of experiments done in this research. The first type involved a Laser Doppler Vibrometer to measure the vibrations on the bottom surface of the robot to analyse the attenuation of the metachronal wave. The second type are velocity experiments, to quantify the locomotion abilities of the robots.

A. Scanning Laser Doppler Vibrometer

The sensor head (OFV 505, Polytec) of the vibrometer is mounted on an aluminum frame at a height of 1 meter from the table on which the frame is fixed. In front of the sensor head, a galvanometer (ScannerMAX Compact 506 Dual Axis Galvanometer, Edmund Optics) is mounted, which can redirect the laser beam of the vibrometer by rotating the two mirrors of the galvanometer. The two motors that drive these mirrors are driven by sending signals through a DAQ (NI USB-6215, National Instruments) to the Mach-DSP servo driver. This driver transfers two voltages, one for the x- and one for the y-component of the location, to a (x,y) location in mm on the table on which the vibrometer is mounted. For each individual scan, first the laser is pointed to the correct location by sending the corresponding signal to the galvanometer, then the measurement starts where the vibrometer controller (OFV 5000, Polytec) measures the vibrations while the signals are sent to the actuators, which is done through the DAQ described in subsection III-A The goal of the experiments with the vibrometer is to visualize how the bottom surface reacts to the sequence of vibrations. For all the experiments a piece of reflective tape is put on the surface that is being scanned, to improve the measurement accuracy of the vibrometer. Multiple different scans can be done, each one with a different purpose.
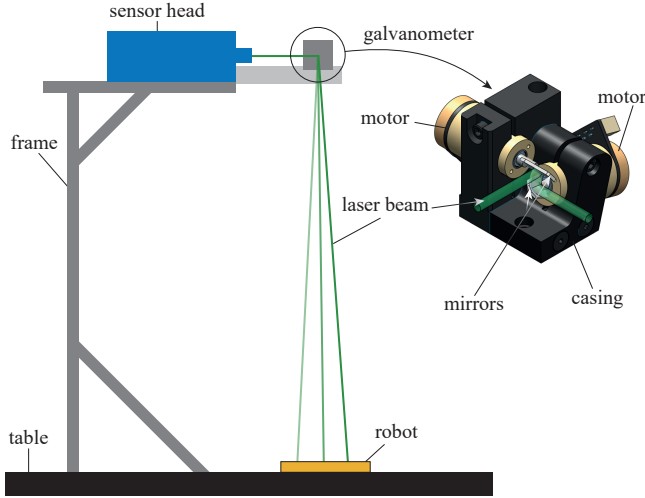
Fig. 8. **Schematic of the Scanning Laser Doppler Vibrometer.** The sensor head of the vibrometer is mounted on top of a frame on a table. In front of the sensor head the galvanometer is mounted, which redirects the laser over the robot by rotating the two mirrors inside the galvanometer.
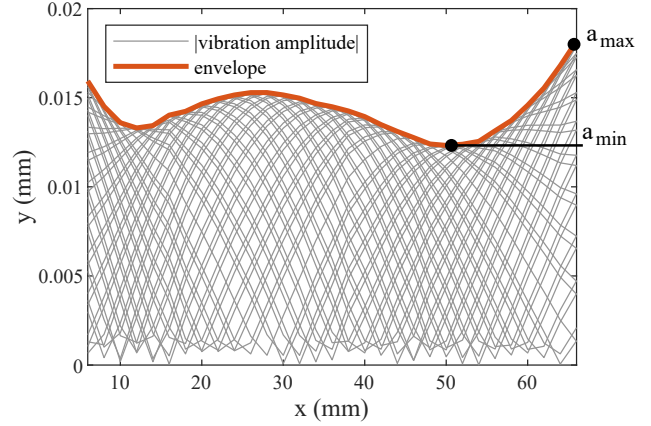

Fig. 9. **Extraction of minimum and maximum values of the vibration amplitude to calculate the traveling wave ratio (TWR).** The magnitude of the vibration amplitude along the robot of one period of the wave is visualized in grey between the first and last actuator. Then the envelope (in orange) is taken, which is the maximum vibration amplitude on each location on the robot. This data set is from the TPU robot with input $f = 235\ Hz$ and $\varphi = \pi/3$.

The first scan has the goal to generate a bode plot to see what the resonance frequency of each actuator is when mounted on the robot. During this scan, the robot is positioned on top of a piece of foam, and a sweep sine with frequencies between $200Hz$ and $600Hz$ is sent to the actuator that is being scanned. The vibration response of this actuator is measured on its centre. This is repeated for each actuator, to visualize the difference between the individual actuators. Each actuator is solely actuated, to exclude the influence of the actuators next to it. This type of scanning was also used for validating if the relative phase shift between consecutive actuators was the same.

The second type of scan is a line scan. During this scan, the robot is upside down on top of a piece of foam, to measure the reaction on the bottom of the robot. The actuators are sent a signal according to Equation 1. The vibration response is then measured along the center line of the robot. These scans are used to visualize the resulting metachronal wave and extract the properties of this wave to compare it to the model.

The third type of scan is a surface scan. This scan is similar to the line scan, but now the full bottom surface of the robot is scanned. This is mainly to visualize the effects of the vibrations, not only along the center line, but also on the edges of the robot.

B. Traveling Wave Ratio

To give a qualitative measure to the propagation of the metachronal wave in the three materials we look at the traveling wave ratio (TWR). The TWR indicates how much of the resulting wave, which is a superposition between multiple standing and traveling waves, is actually a traveling wave. The TWR gives a value between 0, for a pure standing wave, and 1, for a pure traveling wave. The TWR is the inverse of the standing wave ratio (SWR), which can be estimated by calculating the rate of the maximum amplitude divided by the

minimum amplitude of the superposition of waves through a medium. This gives the following formula for the TWR:

$$TWR = \frac{a_{min}}{a_{max}} \tag{12}$$

The vibration amplitudes are extracted from the line scans of the scanning vibrometer as shown in Figure 9. Here, the magnitude of the vibration amplitude of one period of the metachronal wave is visualized between the first and last actuator of the robot. The ends are extracted, to exclude the effects on the edge of the beam. Then the envelope of the vibration amplitude is extracted, visualized in the figure in orange. The TWR is then calculated from the minimum and maximum amplitudes of this envelope.

C. Velocity Experiments

The velocity of a robot was measured to find the influence of different metachronal waves on the locomotion ability of the robot. During each velocity experiment, the robot was placed on a table underneath a smartphone (OnePlus Nord), mounted on a tripod. With the smartphone, each trial of the robot was filmed. This footage is later used to extract the pathway of the robot, from which the velocity could be derived. During each trial, the robot was first sent a set of signals with a fixed frequency and a certain negative phase shift of magnitude φ. Then the robot was sent no signal for 1 second, then a set of signals for 10 seconds with the same frequency and amplitude, but now with positive phase shift φ. This is repeated 3 times for each phase shift φ. To summarise, the result is one video for each metachronal wave with a certain wavelength λ, resulting from the phase shift φ, where the robot moves forward and backward 3 times.

V. RESULTS

A. Damping and Spacing between actuators

From the model we find that a minimal wavelength is desirable for the fastest locomotion speed, as can be seen in Figure 4. To achieve a minimal wavelength, the spacing δ should also be minimized. Since a vibration on a soft material induces a damped traveling wave through that material, the actuators cannot be too close together, otherwise these traveling waves would interfere with each other and induce unwanted deformations along the robot.

To find the minimal required spacing to avoid wave interference, the damping of the vibration was investigated with a long silicone slab with dimensions $l \times w \times h = 400 \times 14 \times 8\ mm$ and one actuator located on one edge. This actuator was sent a sine signal of frequency $f = 250\ Hz$, which is the resonance frequency, and the resulting vibrations over the centre were measured from the actuator at $x = 0\ mm$ to a length of $x = 180\ mm$. One period of the resulting traveling wave is shown in Figure 11 with the envelope of the vibration in orange. Since the wave amplitude was reduced by $2/3$ at $x = 12\ mm$, the spacing between actuators was chosen at $\delta = 12\ mm$.
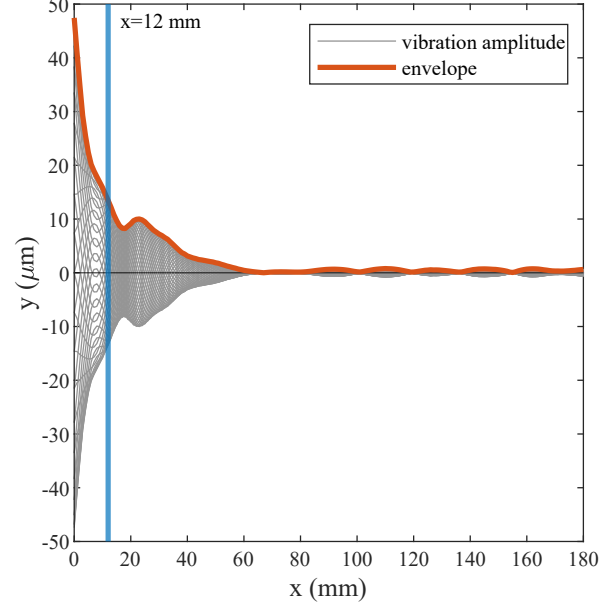

Fig. 11. **Damping of a vibration in silicone.** The results of a vibrometer scan along a slab of silicone with a vibration at $x = 0\ mm$ of $f = 250\ Hz$. In grey the vibration amplitude along the centre line of the silicone slab for different time steps is visualized with in orange the envelope of the resulting wave. At $x = 12\ mm$ the amplitude of the traveling wave is reduced by $2/3$.

B. Validation of Metachronal Wave

With the spacing chosen, the model can be tested to see if a sequence of vibrations indeed induces a metachronal wave that changes according to the model. The results of the line scans along the three robots for various phase shifts are shown in Figure 10. In this figure, the vibrations over the centre line are measured with the scanning vibrometer to see how the curvature of the robot changes over time as a result of the series of vibrations with frequency $f = 250\ Hz$ for the silicone robot and $f = 235\ Hz$ for the rubber and TPU robots. As expected, a phase shift of $\varphi = \pi$ results in a standing wave, which is visible in all three materials. Also according to the model does the positive phase shift result in a metachronal wave traveling to the left and a negative phase shift result in a wave traveling to the right. On top of that, the wavelength of the resulting metachronal wave changes with the phase shift φ according to Equation 3.
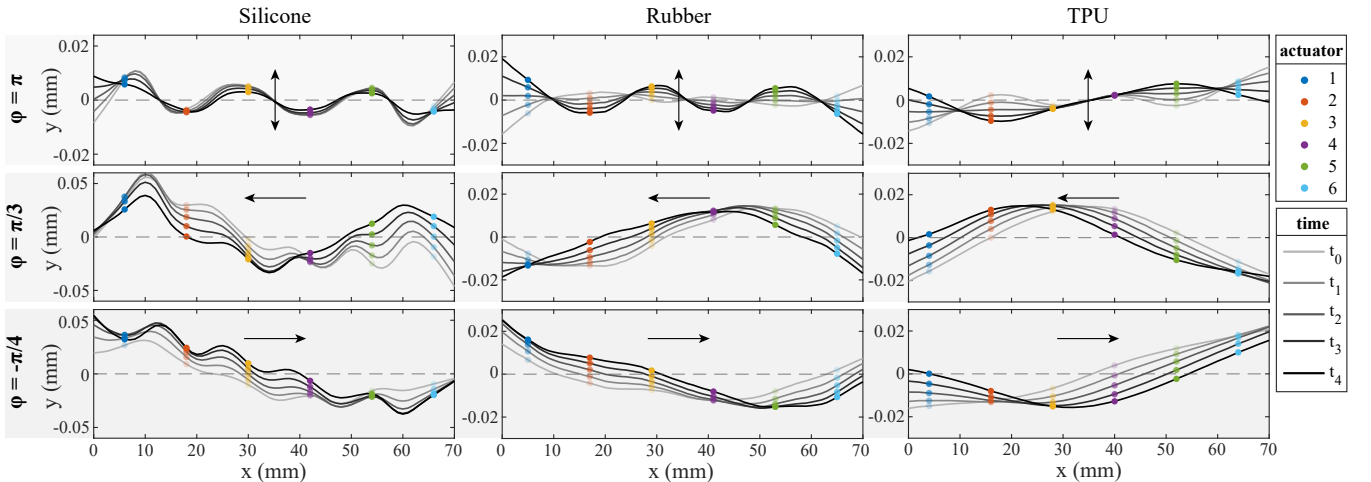

Fig. 10. **Robot centre line curvature for all three robots.** From left to right the curvature along the centre line over time is visualized for the silicone, rubber and TPU robot respectively. Three different phase shifts are shown. On the top a phase shift of $\varphi = \pi$ are shown, where 3 wavelengths are visualized in the robot and a standing wave appears. In the middle the results for a phase shift of $\varphi = \pi/3$ and 1 wavelength along the robot is visualized, with on the bottom the phase shift of $\varphi = -\pi/4$, thus $3/4$ of one wavelength along the robot and the wave traveling to the left instead of the right for the positive phase shifts. The coloured dots represent the 6 actuators and the grey toned lines show the curvature of the robot at different time indices, starting with the lightest shade for the first time step, getting darker each time step.
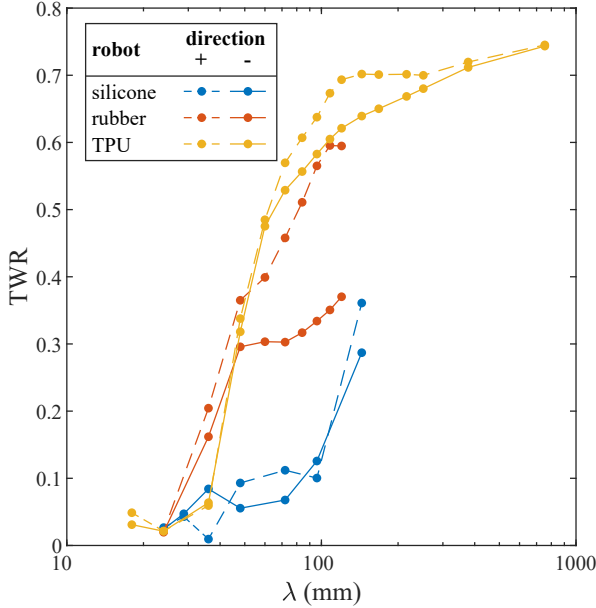
Fig. 12. **The traveling wave ratio (TWR) for different wavelengths in three materials.** The TWR is depicted for forward traveling waves (+) and backward traveling waves (-). The exact values can be found in Appendix C.

Fig. 13. **Measured velocity vs estimated velocity of the TPU robot with frequency $f = 235\,Hz$.** The velocity is estimated according to Equation 11, with the amplitude from the vibrometer data and height $h = 10\,mm$, which is the total height of the robot with actuators on top.

C. Traveling Wave Ratio

To evaluate the attenuation of the different metachronal wave through the three robots the TWR is calculated from the line scan data with the vibrometer. The ratios for different metachronal waves are plotted for all three robots against the wavelength of that metachronal wave in Figure 12. A table for each robot with the TWR values together with the phase shift φ of the input sequence, the wavelength λ of the resulting metachronal wave and the average amplitude can be found in Appendix C.

D. Robot Velocity

The velocity experiments consisted of making videos of the TPU robot with different metachronal waves to extract the velocity. Each input sequence had frequency $f = 235\,Hz$ and phase shifts between .1 and $2\pi/3$, both positive and negative. A MATLAB algorithm is used to extract the locations of the 6 actuators in each video frame to get the pathway of the robot for that specific input. This algorithm is explained in Appendix E and the results are plotted in Appendix F.

In Figure 13 the results of the velocity experiments are plotted together with the modeled velocity. The maximum velocity of the robot was found to be with input phase shift $\varphi = \pi/5$, which results in a metachronal wave with wavelength $\lambda = 120\ mm$. The locomotion pattern of the robot with this input is visualized in Figure 14, where the orientation of the robot at the start and end is visualized with the pathway of the centre of mass. With a positive phase shift the robot moves mostly forward in positive x direction, but with a slight rotation. With a negative phase shift the robot moves backwards to the original position of the robot, again with a small rotation.
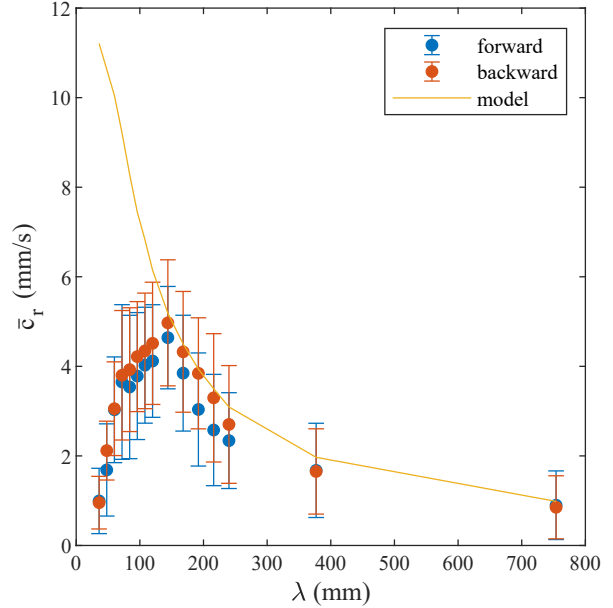
VI. DISCUSSION

A sequence of vibrations with a phase shift can induce a metachronal wave on a robot made from silicone, rubber and TPU. The metachronal wave is a sampled version of a traveling sine wave and its wavelength can be increased both by increasing the spacing between the vibrating actuators and decreasing the phase shift of the vibration between two consecutive actuators, as the model indicated. The rubber and TPU robot were both able to move forward and backward, depending on the sign of the phase shift.

A. Wave Propagation in Soft Materials

The material of the soft robot influences the propagation of the metachronal wave, as can be seen in Figure 10. Here, the centre line curvature of the robots made from silicone, rubber and TPU are shown for three different input sequences with phase shift $\varphi = \pi$, $\pi/3$ and $-\pi/4$. Following the model, there appears a standing wave with $\varphi = \pi$, a backward traveling wave with the positive phase shift, and a forward traveling wave with the negative phase shift. However, the amplitude of the curvature is different in the three materials, as is the smoothness of the curvature. Especially in silicone, the curve between actuators shows a dip, while in rubber and TPU the line is more straight and closer to the model. This can be explained by the higher damping coefficient of silicone compared to rubber and TPU. This might be improved by reducing the spacing δ for the silicone robot or using a actuator with a higher amplitude vibration.

To qualitatively compare the curvature in the three materials the TWR is calculated for each input sequence and plotted over the wavelength of the resulting metachronal wave in
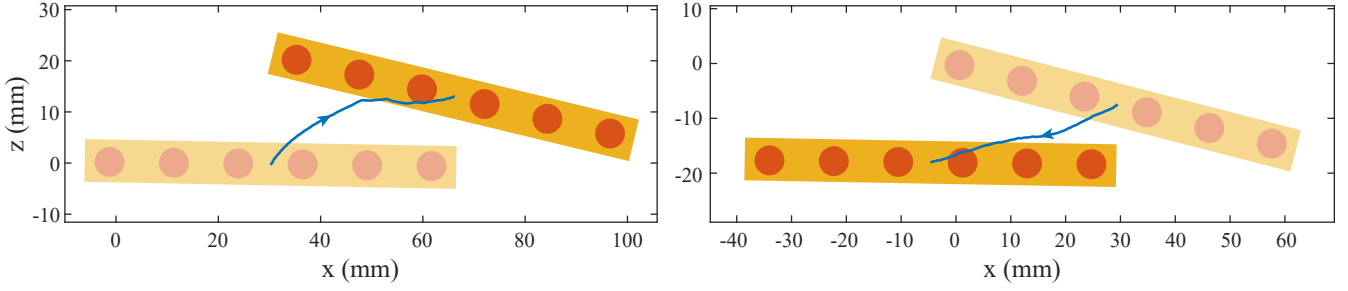
Fig. 14. **The locomotion pattern of the TPU robot** with input signals of frequency $f = 235\,Hz$ and wavelength $\lambda = 120\,mm$ with phase shift $\varphi = \pi/5$. On the left the forward pathway of the centre of mass (CoM) of the robot is visualized, with the initial position of the robot in light shading and the final position of the robot in full colour. In this case the phase shift is negative. The right figure shows the CoM pathway of the backwards traveling robot with a positive phase shift.

Figure 12. It is immediately clear from this figure that the TWR is closer to one for the rubber and TPU robot, which means that the robot curvature for that wavelength mainly consists of traveling waves. In contrast the robot curvature in silicone is closer to zero, which means that more of the curvature consists of standing waves.

In addition, the figure also shows that the TWR improves with increasing wavelength in all three materials. This is likely due to the sampling of the wave, which changes with the wavelength. Since the wavelength of the metachronal wave in the experiments is defined by the phase shift φ of the input sequence and the spacing δ is equal over all experiments. Specifically, the robots have a total length of $72\,mm$ and have 6 actuators, thus 6 points that are sampled of the metachronal wave. When the wavelength is equal to $72\,mm$ (which is for phase shift $\varphi = \pi/3$), exactly 6 points are used to sample the wavelength. When the wavelength increases these 6 points will cover a smaller part of the wavelength, which means that the final metachronal wave will more closely imitate the desired traveling wave and this results in a higher TWR. When the wavelength decreases, less points are used to sample one wavelength, which results in a TWR closer to zero. When the wavelength is $\lambda = 24\,mm$, the phase shift is $\varphi = \pi$ and the curvature of the robot follows a standing wave and the TWR is very close to zero.

The effect of the wavelength and the sampling of the metachronal wave can be further investigated by doing experiments with robots with varying amount of actuators. When multiple robots with the same spacing, but different amount of actuators are made, the sampling of the wave can be investigated separately of the effect of the wavelength.

B. TWR and Robot Velocity

The magnitude of the velocity of the TPU robot follows the trend of the model from a wavelength of $\lambda = 120\,mm$ and phase shift $\varphi = \pi/5$ at the maximum velocity of $5\,mm/s$ and for increasing wavelengths, where the robot velocity slowly decreases towards zero. However, the velocity decreases for smaller wavelengths, contrary to the exponential increase of the velocity in the model. To explain the origin of this effect, we look again at the propagation of a metachronal wave with different wavelengths through the TPU robot. More
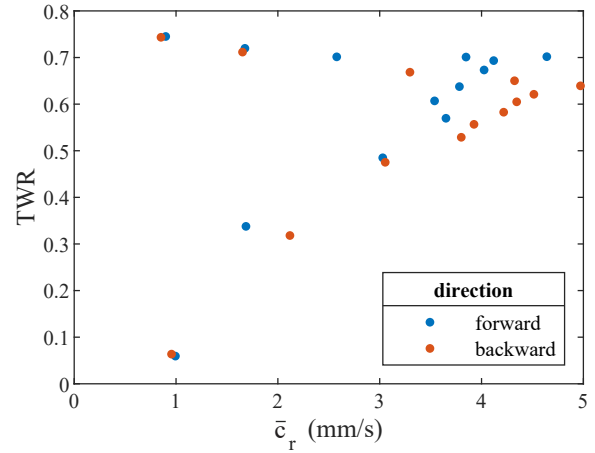

Fig. 15. **Traveling wave ratio (TWR) versus the average robot velocity** for both forward and backward locomotion of the TPU robot.

specifically, the hypothesis that with a smaller wavelength less points are sampled in one wavelength, which is then visible in a TWR that is closer to 0. The TWR is plotted against the average velocity for the TPU robot in Figure 15, where the relation between the TWR and the velocity is clearly visible. Since a low TWR did not result in a high robot velocity. This doesn't necessarily mean that the velocity is always high when the TWR is too, since a larger wavelength results in a high TWR, but a lower velocity, as shown in Figure 13.

The relation between the wave propagation and robot velocity can be further investigated by conducting velocity experiments with robots with varying amounts of actuators, to separate the effect of the sampling and the effect of the wavelength. This way, also the effect of multiple wavelengths in one robot can be investigated compared to lesser wavelengths in a robot with the same spacing and input sequences, but different amount of sampling points or actuators.

Given that the robot velocity closely follows the model when the TWR is above 0.6 and the modeled velocity assumes no slip, the robot might also experience little slip. Although more research has to be done to proof the robot indeed experiences very little slip.

C. Locomotion Path of TPU Robot

The locomotion path of the TPU robot is not a straight line along the x-axis like the model, but is a curved path, see Figure 14. The robot rotates during forward locomotion, and rotates back to the original position during backwards locomotion. There can be multiple explanations for this rotation. First of all, the small amplitude of the vibration can only impose a small forward force on the robot. This small force is easily affected by external factors, like the tension in the wires that connect the actuators to the amplifiers. This tension puts a force on the robot that is perpendicular to the direction of motion. This force acts like a centripetal force and could have caused the robot to move along a circular path.

Furthermore, the amount of cycles of the wave that deform the robot can have an influence. For example, the phase shift $\pi/3$ causes exactly one cycle of the wave in the robot with wavelength $\lambda = 72 \ mm$, which is the same as the length of the robot. With one cycle of the wave only one point on the bottom of the robot actually moves the robot forward, and is at the bottom of the ellipsoidal motion like in Figure 3a. According to the model, the other points along the bottom of the robot shouldn't be touching the ground. However, it is not certain that only one point of the robot was touching the surface at all times, since the amplitude of the motion is around $20 \ \mu m$. Thus $20 \ \mu m$ is also the furthest distance between the feet and the ground, which is so small that it could be possible that other points are touching the ground too. These other point may have acted as an anchor for the robot to rotate around. Further investigation is needed to fully investigate if this is the case, for example by capturing the motion of the bottom of the robot with a high speed camera.

D. Possible Inconsistencies with Vibrometer Measurements

The extra layer of reflective tape on top of the robots for the vibrometer measurements may have influenced the results. The reflective tape was put on the bottom of the robot to increase the accuracy of the vibrometer measurements. Without the tape the measurements could not be done, because the laser signal used to measure the velocity of the vibration would not be reflected back into the laser head of the vibrometer, but instead would be scattered around or absorbed by the robot.

The tape also did not adhere well to silicone, which might have influenced the vibrometer measurements with the silicone robot. It would stick a little bit, but detach each time the robot was moved. The robot needed to be moved to be properly aligned with the axis system of the scanning vibrometer. All this movement may have led to small air pockets between the silicone and the tape. The detachment of tape did not happen with the rubber and TPU robots, where the tape remained attached when the robot was moved.

On all robots the tape might have amplified the vibration measured on the edges. At the edges, the tape did not stick as well and acted as a free end of the beam, which might have led to higher vibration amplitudes on the ends compared to the centre. The amplification due to the free end beam behavior of the tape added to the free end beam behavior that is already present, at the edges of the robot itself.

E. Effect of Feet on locomotion

The TPU robot was given feet to increase the height of the robot without losing its ability to deform with the metachronal wave. The increase in height is desirable, since the model shows that this would increase the velocity of the robot as well, see Equation 11. However, the feet on the TPU robot might influence the attenuation of the vibration through the robot, since the attenuation of the vibration is disrupted when it reaches the empty spaces between the feet. The effect of this disruption on the propagation of the metachronal wave and with that the locomotion of the robot is not known, since only the vibrations at the bottom of feet can be measured with the vibrometer and only one robot with feet is analysed.

More research needs to be done into the effect of the feet on the propagation of the metachronal wave and its relation to the locomotion abilities of the robot. This can be investigated by looking at robots with the same outside dimensions, but different variations of feet. Also the effect of changing the dimensions of the feet themselves or the amount of feet can be researched and optimized for locomotion.

F. Actuation

The robots in this research used linear resonant actuators as a vibration source. These actuators have little power requirements, work with an AC input, and are small in size. These actuators fulfilled all requirements for a proof of concept, but also came with some disadvantages.

First of all, linear resonant actuators are very frequency dependent. The amplitude of the vibration drastically decreases when the vibration frequency gets further away from the resonance frequency. Therefore, each robot could only be tested with one frequency. This frequency was also different for each robot, since the material of the robot and the placement of the actuator influenced the resonance of the system and with that the resonance of the actuator itself. Additionally, there were individual differences between how each actuator reacted to a vibration signal, which led to differences in vibration amplitude between the actuators. These variations in vibration amplitude could have reduced the TWR, which was calculated by dividing the minimum vibration amplitude along the bottom of the robot by the maximum vibration amplitude, since this maximum amplitude could not be achieved by each actuator.

Another downside to linear resonant actuators is the small vibration amplitude. Since the robot velocity is proportional to the vibration amplitude. Further research needs to be done into vibration sources with a higher vibration amplitude and preferable, a wider frequency range as well. Since a wider frequency range would lead to lesser differences between the vibration amplitudes of individual actuators.

G. Scalability of the Robot

A second type of linear resonant actuator (LRA12235L, GREWUS) was used to investigate the scalability of the robot. With these larger actuators, two TPU robots with 6 actuators and spacing $\delta = 20 \ mm$ and $\delta = 30 \ mm$ were made. Both robots were able to generate metachronal waves, but these waves did not result in controllable locomotion. A detailed

explanation of this research can be found in Appendix D. Although the robots with the large actuators did not move according to the model, the research did provide some key insights into what to take into account when designing a soft robot that generates metachronal waves for locomotion.

Similar to the actuators in the main research, these larger actuators also showed individual differences in response to signals. However, with the larger actuators not only the amplitude would differ from actuator to actuator, also the phase of the resulting signal showed large differences. This is clearly visible in Figure D.3, where the bode plot of each actuator showed significant differences both in magnitude and phase.

Secondly, the surface scans of both TPU robots with large actuators shows that the wave travels at an angle, see Figure D.5 and D.6. This may have caused the robot to rotate even more than the robot with the smaller actuators. The cause of this angled wave propagation is not exactly known. It might be caused by inconsistencies in the 3D print of the robot or the placement of the actuators.

The advancement ratio (AR) [11] gives another reason to the contrast in locomotion abilities. The AR is the ratio between robot velocity and wave velocity, which with my model is equal to $AR = \frac{\bar{c}_r}{c_w} = a\frac{h}{2}(\frac{\varphi}{\delta})^2$. Calculating this ratio for both robots with phase shift $\varphi = \pi/5$, gives $AR_{smallLRA} = 2.2 \times 10^{-4}$ and $AR_{largeLRA} = 8.8 \times 10^{-5}$. This difference in AR is due to the larger spacing needed for the robot with the large actuators, which is not compensated enough by the increased robot thickness h and the small increase in vibration amplitude a. Although both values for the AR are small, the 10 fold smaller AR for the robot with larger actuators might be too small to push forward the heavier robot.

Furthermore, the 3D printer might have influenced the larger robots more than the first smaller TPU robot. There were visible differences in quality between the robots; the first robot is straight and printed consistently, while the larger robot had a slight curve when not actuated, which caused some of the feet to levitate instead of touching the ground. This curvature may have been caused by the 3D printer, since the quality of the print is influenced by both the environment and the settings of the printer. Not only the surrounding temperature and moisture levels of the space where the 3D printer is located have an effect on the quality, but also the settings for the 3D print like the wall thickness, the infill and the velocity of the printer. Especially the ratio between wall and infill of the robot might have impacted the difference in quality and locomotion abilities, since the wall thickness of the 3D print was the same for both robots, while the outer dimensions are larger for the larger robot, which might have effected the propagation of the metachronal wave. Further research can be done into what 3D printer settings work best for soft robots of different sizes and maybe also into other soft materials that can be 3D printed that result in higher quality prints with lesser inconsistencies.

Further research needs to be done into which of the issues stated above played a role and how they can be overcome to make a larger robot move with metachronal waves.

H. Future Recommendations

The research proposed here will help with the development of an untethered soft robot with a large range of motion. Before this goal is reached for the robot in this research, first the capabilities of the robot need to be improved by for example increasing its vibration amplitude and making its locomotion path more straight. Then more research into its weight carrying abilities can be done to investigate how the design of the robot can be changed to be able to carry equipment and lose the tether to the amplifiers. A solution for minimizing the equipment needed for the robot is by imposing the phase shift between the actuators through hardware instead of software. This way, only one signal needs to be generated and amplified, which reduces the amount of hardware the robot needs to carry.

The idea of using a sequence of vibrations to generate a metachronal wave can also be used for other purposes besides locomotion. For example, the actuators can be put in a grid where a metachronal wave can be generated in all directions over this grid. These can then be used for directional cues and haptic feedback in soft surfaces.

VII. Conclusion

A soft robot can use a sequence of vibrations to generate a metachronal wave for bidirectional locomotion. The wavelength of the metachronal wave can be changed both by increasing the spacing between consecutive actuators and by reducing the phase shift between consecutive vibrations. The soft robot proposed in this research is able to move at a speed of $5\ mm/s$. The robot has a simple design and since the robot accurately follows the model at high TWR, faster velocities could be reached when the vibration amplitude is increased. This research provides a step into making a soft robot that can not only move efficiently, but also has a wide range of motion which can bring it almost anywhere.

Acknowledgment

References

[1] G. M. Whitesides, "Soft Robotics," *Angewandte Chemie International Edition*, vol. 57, no. 16, pp. 4258–4273, 4 2018. [Online]. Available: http://doi.wiley.com/10.1002/anie.201800907

[2] M. Calisti, G. Picardi, and C. Laschi, "Fundamentals of soft robot locomotion," *Journal of The Royal Society Interface*, vol. 14, no. 130, p. 20170101, 5 2017. [Online]. Available: https://royalsocietypublishing.org/doi/abs/10.1098/rsif.2017.0101https://royalsocietypublishing.org/doi/10.1098/rsif.2017.0101

[3] M. Watanabe and H. Tsukagoshi, "Soft sheet actuator generating traveling waves inspired by gastropod's locomotion," in *2017 IEEE International Conference on Robotics and Automation (ICRA)*. IEEE, 5 2017, pp. 602–607. [Online]. Available: http://ieeexplore.ieee.org/document/7989074/

[4] ——, "Flexible Sheet Actuator That Generates Bidirectional Traveling Waves," *2018 IEEE/ASME International Conference on Advanced Intelligent Mechatronics (AIM)*, vol. 2018-July, pp. 328–333, 7 2018. [Online]. Available: https://ieeexplore.ieee.org/document/8452700/

[5] L. Salem, A. D. Gat, and Y. Or, "Fluid-Driven Traveling Waves in Soft Robots," *Soft Robotics*, vol. 00, no. 00, pp. 1–10, 2 2022. [Online]. Available: https://www.liebertpub.com/doi/10.1089/soro.2021.0116

[6] M. T. Tolley, R. F. Shepherd, B. Mosadegh, K. C. Galloway, M. Wehner, M. Karpelson, R. J. Wood, and G. M. Whitesides, "A Resilient, Untethered Soft Robot," *Soft Robotics*, vol. 1, no. 3, pp. 213–223, 2014.

[7] W. Hu, G. Z. Lum, M. Mastrangeli, and M. Sitti, "Small-scale soft-bodied robot with multimodal locomotion," *Nature*, vol. 554, no. 7690, pp. 81–85, 2 2018. [Online]. Available: http://www.nature.com/articles/nature25443http://www.nature.com/articles/nature25443

[8] V. K. Venkiteswaran, L. F. P. Samaniego, J. Sikorski, and S. Misra, "Bio-Inspired Terrestrial Motion of Magnetic Soft Millirobots," *IEEE Robotics and Automation Letters*, vol. 4, no. 2, pp. 1753–1759, 4 2019. [Online]. Available: https://ieeexplore.ieee.org/document/8636997/

[9] M. Kuribayashi, S. Ueha, and E. Mori, "Excitation conditions of flexural traveling waves for a reversible ultrasonic linear motor," *Journal of the Acoustical Society of America*, vol. 77, no. 4, pp. 1431–1435, 1985.

[10] C. Majidi, R. F. Shepherd, R. K. Kramer, G. M. Whitesides, and R. J. Wood, "Influence of surface traction on soft robot undulation," *The International Journal of Robotics Research*, vol. 32, no. 13, pp. 1577–1584, 11 2013. [Online]. Available: http://journals.sagepub.com/doi/10.1177/0278364913498432

[11] D. Zarrouk, M. Mann, N. Degani, T. Yehuda, N. Jarbi, and A. Hess, "Single actuator wave-like robot (SAW): Design, modeling, and experiments," *Bioinspiration and Biomimetics*, vol. 11, no. 4, p. 046004, 7 2016. [Online]. Available: https://iopscience.iop.org/article/10.1088/1748-3190/11/4/046004https://iopscience.iop.org/article/10.1088/1748-3190/11/4/046004/meta

[12] PrecisionMicrodrives, "Linear resonant actuators," https://www.precisionmicrodrives.com/linear-resonant-actuators-lras, 2021, accessed: 1-10-2022.

APPENDIX A
ROBOT VELOCITY ESTIMATION

The velocity of the robot is equal in value and opposite in sign to the instantaneous velocity at a point p on the bottom of the robot that is in contact with the ground [11]. The transverse displacement of the robot is equal to the metachronal wave:

$$v(x,t) = a\sin(\omega t + kx), \qquad k = \frac{\varphi}{\delta}$$

And the longitudinal displacement is equal to [9]:

$$u(x,y,t) = -y\frac{\partial v}{\partial x} = -a\frac{h}{2}k\cos(\omega t + kx)$$

This gives the following equation for the robot velocity:

$$c_r(t) = -\dot{x}_p(t) = -\frac{\partial u}{\partial t} = a\frac{h}{2}k\omega\sin(\omega t + kx_p)$$

At the contact point x_p the derivative of the transverse displacement is equal to zero:

$$\frac{\partial v}{\partial x_p} = ak\cos(\omega t + kx_p) = 0$$

To solve this equation for x_p, we used the following trigonometric formula:

$$\cos(\alpha + \beta) = \cos(\alpha)\cos(\beta) - \sin(\alpha)\sin(\beta),$$

which gives:

$$\cos(\omega t)\cos(kx_p) - \sin(\omega t)\sin(kx_p) = 0,$$

$$\frac{\cos(\omega t)}{\sin(\omega t)} = \frac{\sin(kx_p)}{\cos(kx_p)}, \qquad \tan(kx_p) = \frac{\cos(\omega t)}{\sin(\omega t)},$$

$$x_p = \frac{1}{k}\tan^{-1}\left(\frac{\cos(\omega t)}{\sin(\omega t)}\right)$$

Now we have an equation for the contact point x_p, we can implement this into the formula for the robot velocity:

$$c_r(t) = a\frac{h}{2}k\omega\sin\left(\omega t + \tan^{-1}\left(\frac{\cos(\omega t)}{\sin(\omega t)}\right)\right)$$

To simplify this equation, we use the inverse trigonometric functions:

$$\sin(\tan^{-1}(x)) = \frac{x}{\sqrt{1+x^2}}, \quad \cos(\tan^{-1}(x)) = \frac{1}{\sqrt{1+x^2}}$$

For easier reading, we say that $A = \frac{\cos(\omega t)}{\sin(\omega t)}$. Implementing the inverse trigonometric functions together with the trigonometric function from before into the robot velocity function will simplify the equation as follows:

$$c_r(t) = a\frac{h}{2}k\omega\left(\sin(\omega t)\cos(\tan^{-1}(A)) + \cos(\omega t)\sin(\tan^{-1}(A))\right) =$$
$$a\frac{h}{2}k\omega\left(\sin(\omega t)\frac{1}{\sqrt{1+A^2}} + \cos(\omega t)\frac{A}{\sqrt{1+A^2}}\right) =$$
$$a\frac{h}{2}k\omega\left(\frac{\sin(\omega t) + A\cos(\omega t)}{\sqrt{1+A^2}}\right)$$

Replacing A again gives:

$$c_r(t) = a\frac{h}{2}k\omega\left(\frac{\sin(\omega t) + \cos(\omega t)\frac{\cos(\omega t)}{\sin(\omega t)}}{\sqrt{1+\frac{\cos^2(\omega t)}{\sin^2(\omega t)}}}\right) =$$
$$a\frac{h}{2}k\omega\left(\frac{\sin^2(\omega t) + \cos^2(\omega t)}{\sin(\omega t)\sqrt{1+\frac{\cos^2(\omega t)}{\sin^2(\omega t)}}}\right)$$

Since $\sin^2(\omega t) + \cos^2(\omega t) = 1$ and

$$1 + \frac{\cos^2(\omega t)}{\sin^2(\omega t)} = \frac{\sin^2(\omega t) + \cos^2(\omega t)}{\sin^2(\omega t)} = \frac{1}{\sin^2(\omega t)},$$

we get the following formula for the robot velocity over time:

$$c_r(t) = a\frac{h}{2}k\omega\left(\frac{1}{\sin(\omega t)\sqrt{\frac{1}{\sin^2(\omega t)}}}\right)$$

Thus, the average robot velocity becomes:

$$\bar{c}_r = \frac{1}{T}\int_0^T c_r(t)dt = \frac{1}{T}\int_0^T a\frac{h}{2}k\omega dt = a\frac{h}{2}k\omega$$

APPENDIX B
SCANNING LASER DOPPLER VIBROMETER

To give the laser doppler vibrometer (LDV) in the lab the ability to scan surfaces, we designed a frame with a galvanometer to move the laser over an object. With this setup, the velocity of vibrations on surfaces can be measured and visualized. In this appendix all the components of the scanning vibrometer are described, starting with the physical components and the design of the frame, and ending with a description how to control the scanning of the vibrometer with MATLAB.

Design

The main parts of the scanning vibrometer are the LDV sensor head (OFV 505, Polytec), the LDV controller (OFV 5000, Polytec) and the galvanometer (ScannerMAX Compact 506 Dual Axis Galvanometer, Edmund Optics). To be able to use these components, the sensor head needs to be mounted on top of a frame, with in front of it the galvanometer, which can redirect the laser beam coming from the sensor head to the scanning surface. The galvanometer consists of a little frame with two servomotors attached to two mirrors, in a 90 degree angle from each other. By rotating these mirrors, the beam can be redirected over the ground surface.

In Figure B.1 a picture of the setup in the lab is shown. This setup consists of a frame, which lifts the sensor head and galvanometer to about $1\ m$ above the table. The galvanometer is mounted on a 3D printed pitch yaw system, which is attached to align the galvanometer in a way that the laserbeam will make a 90 degree angle down to the surface, when the galvanometer is in neutral position. This 3D printed system may be replaced by a more robust one from Thorlabs (PY003/M), when it fails. The galvanometer also comes with its own Mach-DSP servo driver and power supplies for both servomotors, which are mounted on top of the frame next to the sensor head.

The frame itself is primarily made out of $30x30\ mm$ aluminium profiles with a $6\ mm$ groove (761-3280, RS PRO), connected together with 3D printed angle brackets for 45 and 90 degree angles. The frame is mounted on a Nexus breadboard table with optimized damping (B60120A, Thorlabs). On this table a PMMA plate with a lasercut grid is mounted, to make it easier to align the surface that needs to be measured with the laser.

Control

The scanning vibrometer is controlled by sending two voltages, one for the x and one for the y coordinate, to the Mach-DSP servo driver that controls the servomotors on the galvanometer. These two voltages dictate where the laser will scan and represent the location on the grid below. They can be calculated as follows:

From the data sheet we know that our Mach-DSP servo driver is set to turn ±20 degrees when the max voltage of $\pm10\ V$ is applied, this makes the conversion factor of the galvanometer $C_{LDV} = 1/2\ (V/degrees)$. To calculate how
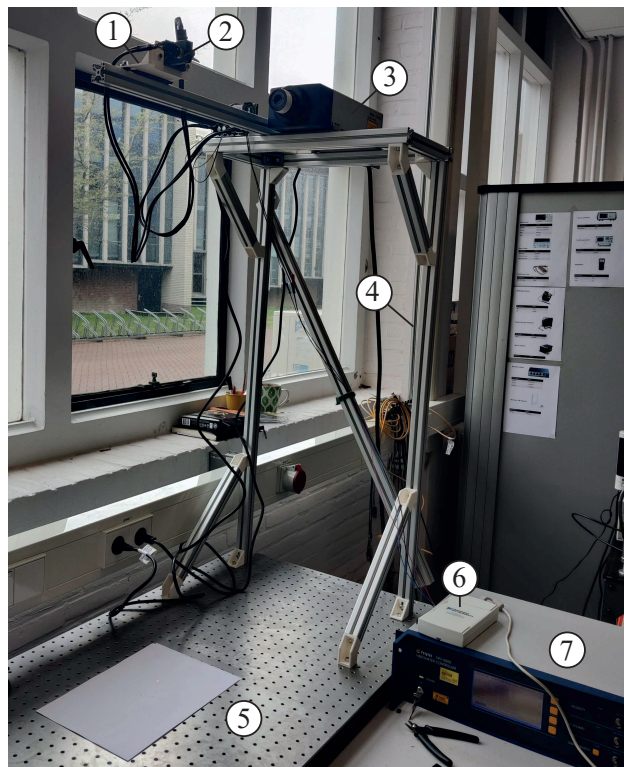

Fig. B.1. **Picture of the scanning laser doppler vibrometer in the lab.** 1. Pitch yaw system 2. Galvanometer 3. Sensor head of vibrometer 4. Frame 5. Table and scanning surface 6. DAQ 7. Controller of the vibrometer

much the voltage needs to be increased for a certain grid step along one axis in (mm) we need to calculate the angle θ that the motor of the corresponding axis needs to make. Since the angles are very small, we use the tangent approximation $\tan(\theta) \approx \theta$, which is then equal to:

$$\theta\,(degrees) = \frac{GridStep\,(m)}{OpticalLength\,(m)} * \frac{360}{2\pi}, \quad (13)$$

where $OpticalLength$ is the distance that the laser travels from the sensor head to the scanning surface. In this setup, this distance for both coordinates is $OpticalLengthX = 1.055 - ObjectHeight$ and $OpticalLengthY = 1.105 - ObjectHeight$, both measured in meters. The $ObjectHeight\,(m)$ is the distance between the Nexus Breadboard table and the scanning surface, or the thickness of the object you measure. Keep in mind that the grid board is $3\,mm$ thick, so add that to the $ObjectHeight$ as well. The voltage needed for every step of size $GridStep\,(m)$ is:

$$GridStep\,(V) = \theta * C_{LDV} = \frac{90 * GridStep\,(m)}{\pi * OpticalLength\,(m)} \quad (14)$$

The voltages needed for steps in x and y direction can both be calculated with Equation 14. Each time the laser needs to be changed direction, you simple send the two voltages through the DAQ board to the motors and the laser will change. With this in mind, any vector or matrix with scanning points along the x y grid can be made and used to measure vibrations along the surfaces.

In this appendix an overview of the data from the LDV line scans for all robots is displayed. Each robot got send signals with one frequency, but the vibration amplitude along a line was scanned for different phase shifts φ and thus a different wavelength λ. The resulting data sets give the average amplitude and traveling wave ratio (TWR) for the positive and negative phase shifts, which correspond to backward traveling waves with a positive phase shift and forward traveling waves for a negative phase shift.

TABLE C.1
LINE SCAN RESULTS SILICONE ROBOT WITH FREQUENCY $f = 250\ Hz$

$\varphi\ (rad)$	$\lambda\ (mm)$	Positive		Negative	
		$A\ (\mu m)$	TWR	$A\ (\mu m)$	TWR
π	24	12.08	0.03	12.04	0.02
$5\pi/6$	28.8	13.28	0.04	12.43	0.05
$2\pi/3$	36	18.85	0.01	18.02	0.08
$\pi/2$	48	21.97	0.09	21.17	0.06
$\pi/3$	72	31.20	0.11	29.82	0.07
$\pi/4$	96	29.57	0.10	28.82	0.13
$\pi/6$	144	32.92	0.36	31.63	0.29

TABLE C.2
LINE SCAN RESULTS RUBBER ROBOT WITH FREQUENCY $f = 235\ Hz$

$\varphi\ (rad)$	$\lambda\ (mm)$	Positive		Negative	
		$A\ (\mu m)$	TWR	$A\ (\mu m)$	TWR
π	24	5.48	0.02	5.47	0.02
$2\pi/3$	36	10.25	0.20	10.14	0.16
$\pi/2$	48	11.73	0.37	11.39	0.30
$2\pi/5$	60	12.32	0.40	11.99	0.30
$\pi/3$	72	12.61	0.46	12.25	0.30
$2\pi/7$	84	12.71	0.51	12.36	0.32
$\pi/4$	96	12.75	0.57	12.36	0.33
$2\pi/9$	108	12.75	0.60	12.35	0.35
$\pi/5$	120	12.77	0.59	12.35	0.37

TABLE C.3
LINE SCAN RESULTS TPU ROBOT WITH $f = 235\ Hz$

$\varphi\ (rad)$	$\lambda\ (mm)$	Positive		Negative	
		$A\ (\mu m)$	TWR	$A\ (\mu m)$	TWR
$4\pi/3$	18	8.28	0.05	8.98	0.03
π	24	6.64	0.02	6.63	0.02
$2\pi/3$	36	8.70	0.06	8.05	0.06
$\pi/2$	48	10.96	0.34	10.28	0.32
$2\pi/5$	60	12.97	0.48	12.10	0.48
$\pi/3$	72	14.27	0.57	13.49	0.53
$2\pi/7$	84	14.95	0.61	14.33	0.56
$\pi/4$	96	15.38	0.64	14.91	0.58
$2\pi/9$	108	15.69	0.67	15.32	0.60
$\pi/5$	120	15.90	0.69	15.63	0.62
$\pi/6$	144	16.13	0.70	15.97	0.64
$\pi/7$	168	16.23	0.70	16.13	0.65
$\pi/9$	216	16.27	0.70	16.18	0.67
0.3	251.3	16.24	0.70	16.17	0.68
0.2	377.0	16.13	0.72	16.08	0.71
0.1	754.0	15.99	0.75	15.97	0.74

APPENDIX D
TPU ROBOT WITH LARGE ACTUATORS

In this appendix the research done with a robot with larger actuators is described. This second type of actuator was used since it was available in larger quantities and arrived in 2 days instead of the 2 months waiting time of the smaller actuators. This meant, that research into the scalability of the design and into robots with more than 6 actuators could be done. However, this research did not exactly go as planned, due to complications with the actuators and amplifiers of the system. This resulted in two TPU robots, where metachronal waves are generated, but did not result in controllable locomotion. The robot only rotates, and does not change direction. The research that is done, does give an insight into how the robot behaves as a system and what aspects of the design needs to be considered when designing a larger robot that uses vibrations to generate a metachronal wave for locomotion.

The actuators themselves are linear resonant actuators called LRA 12235L A from GREWUS. They have a diameter of $12.5\,mm$ and heigth of $5.8\,mm$, and require a signal with resonant frequency $235\,Hz$ and RMS amplitude $1.5\,V$, similar to the smaller actuators used in the research described in the main report. Apart from the size, the other difference between the small and large actuators is that instead of the wave spring inside the motor housing of the small actuators, these larger actuators have a spring cut into a metal sheet on top of the housing, as can be seen in Figure D.2.

Two TPU robots are researched, one with spacing $\delta = 20\,mm$ and body dimensions $l \times w \times h = 120 \times 20 \times 9\,mm$ and one with $\delta = 30\,mm$ and body dimensions $l \times w \times h = 170 \times 20 \times 9\,mm$, see Figure D.2. The total height of both robots including the actuators is $14\,mm$.
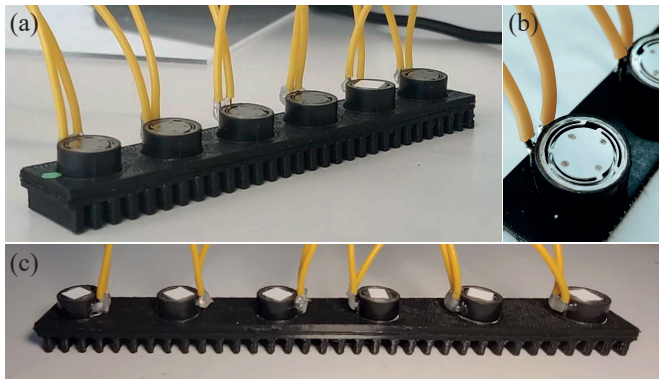

Fig. D.2. **Robots with large actuators** (a) A TPU robot with 6 actuators with spacing $\delta = 20\,mm$. (b) Top view of one of the large actuators with the sheet metal spring on the top of the actuator housing. (c) A TPU robot with 6 actuators and spacing $\delta = 30\,mm$. The silver squares on top of the actuators are pieces of reflective tape to increase the quality of the signal acquired with the vibrometer.

Variance between actuators

The first issue with the larger actuators is the variance between the response of each individual actuator to a signal. When a signal has a certain frequency an no phase shift, each
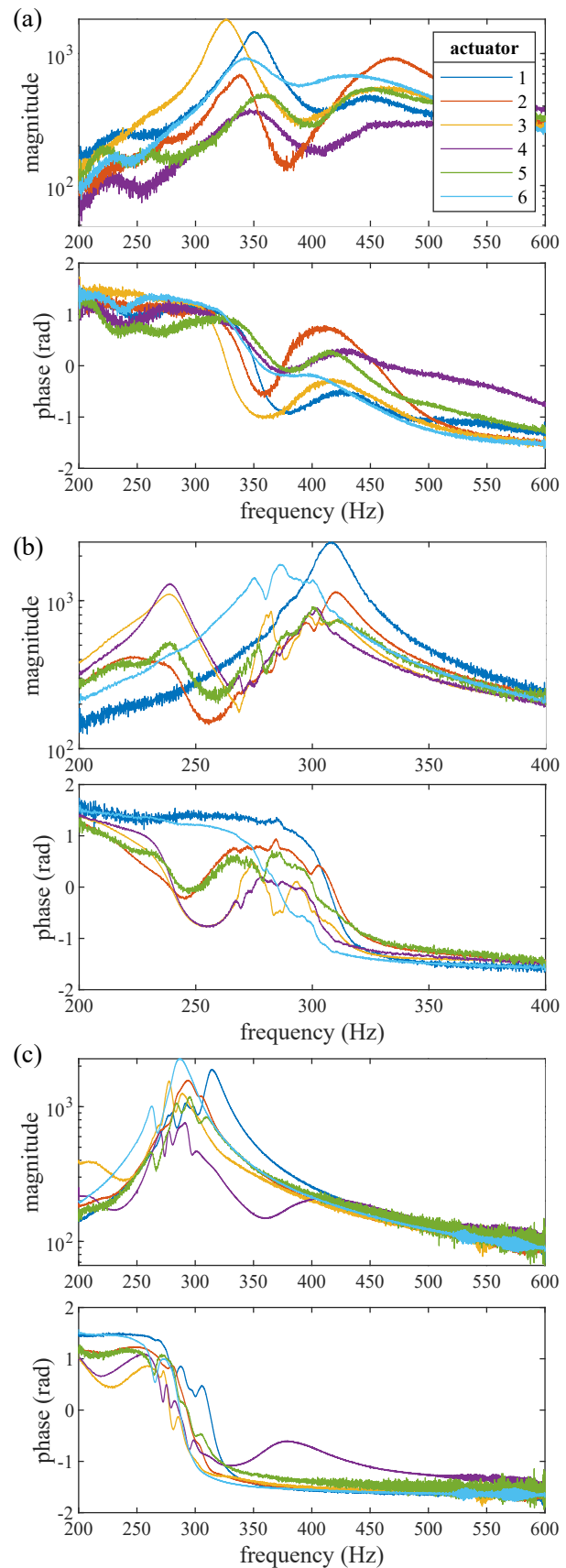

Fig. D.3. **Bode plots of 6 large actuators** Each color represents a different actuator and shows a different response to each frequency. (a) Actuators placed on foam. (b) Actuators on TPU robot with spacing $\delta = 20\,mm$. (c) Actuators on TPU robot with spacing $\delta = 30\,mm$.

actuator response measured with the vibrometer shows a signal with that same frequency, but for each individual actuator a different amplitude and phase. This amplitude difference is not necessarily an issue, since this was also the case with the moving robot from the main paper, but the phase difference is. This meant that the phase shift between consecutive actuators is not fixed anymore.

To find the frequency where the additional phase shift is similar for each individual actuator, the response of each actuator to a sine sweep between $200-600\ Hz$ was measured with the vibrometer. The bode plot from these measurements with the actuators placed on foam and the measurements taken on the two TPU robot with 6 actuators is shown in Figure D.3. There is a clear difference between the bode plots even though they are of the same actuators, since in the first plot, the actuators cannot influence each other due to the foam in between, while in the second and third bode plot they can, since the actuators where all stuck on the same TPU robot.

The performance of the actuators is strongly related to the robot itself. More specifically, the distance between the actuators and the dimensions of the robot together with the material properties of the robot, as described in the main paper, are influencing the resonance frequency of the system. This resonance frequency is not necessarily the best frequency for generating the metachronal wave, since the phase difference between actuators at the resonance frequency results in an unwanted additional phase shift between actuators.

Wave interference

Another complication with the larger actuators is the wave interference between consecutive actuators. In Figure D.4 the envelope of the amplitude response along the robot with $\delta = 20\ mm$ to a signal with frequency $f = 310\ Hz$ is shown for each actuator. Each line represents the response of only one actuated actuator that has the matching color asterisk. There is an overlap between the response of the different actuators, which means that a spacing of $\delta = 20\ mm$ is too small and

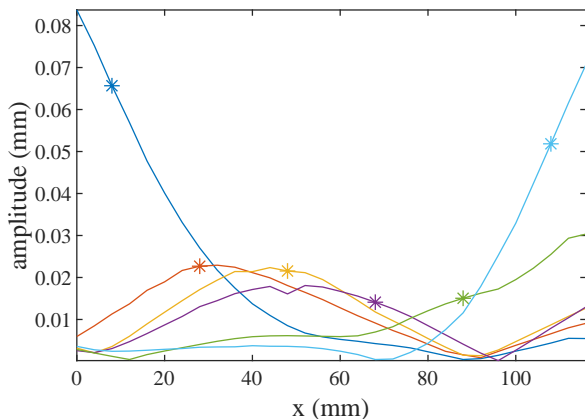Fig. D.5. **Surface scan of TPU robot with 6 big LRA's**, spacing $\delta = 20mm$, and input signals with $f = 325\ Hz$, wavelength $\lambda = 160\ mm$ and $\varphi = \pi/4$. The amplitude in y-direction of the response to this signal is visualized over the full bottom surface of the robot, with the width in z-direction and length in x-direction. The four consecutive time steps are $2.5e-4$ seconds apart.

needs to be increased. This also means that the wavelength of the metachronal wave will be larger and with that a smaller estimated robot velocity. The vibration of the two actuators on the edge show a $2/3$ decrease of amplitude after $20\ mm$, while response of the actuators in the centre overlapped. Here a $2/3$ decrease of amplitude only happened after $40\ mm$. Since the silicone prototype showed damping of the wave between the actuators, the spacing for the next prototype was chosen to correspond with the distance needed for the wave to damp out by $1/2$, which results in a spacing of $\delta = 30\ mm$ for the second prototype with large actuators.

To show the wave propagation along the full bottom surface of the two robots, a surface scan is done with phase shift $\varphi = \pi/4$, which induced 2/3 of one wavelength along the robot, which can be seen in Figure D.5 and D.6. Both visualizations show a wave that is traveling along the bottom in a slight angle. The results for the robot with spacing $\delta = 20\ mm$ in Figure D.5 is more noisy, compared to the robot with larger spacing, due to the reduced spatial resolution of the surface scan.

Results from vibrometer measurements

To show the effect of the frequency on the TPU robot with large actuators, two experiments were done with the robot with spacing $\delta = 30\ mm$. These experiments included two line scans with the vibrometer along the centre line on the bottom of the robot. The first experiment was done with frequency $f = 250\ Hz$ and the second with $f = 350\ Hz$. Both frequencies showed minimal phase difference in the bode plot and had similar magnitudes, see Figure D.3c. Each experiment

Fig. D.4. **Response of each individual actuator on a TPU robot with spacing** $\delta = 20\ mm$ to a vibration with $f = 310\ Hz$. Each * represents the vibrating actuator and the line with the same color shows the amplitude envelope of the vibration response to that same actuator along the robot.
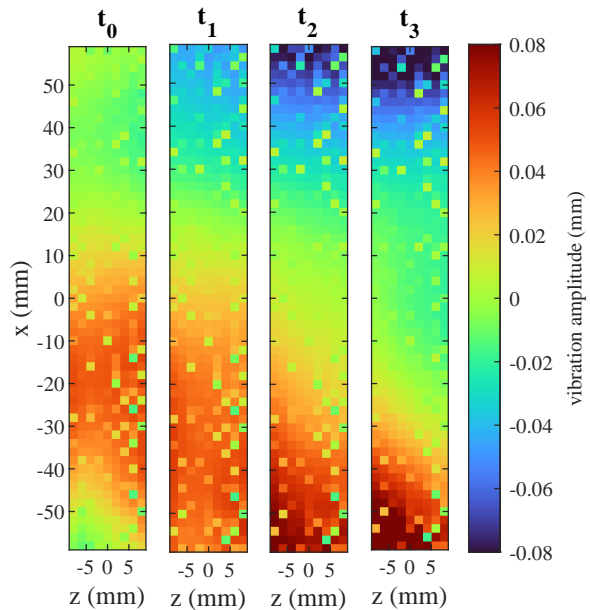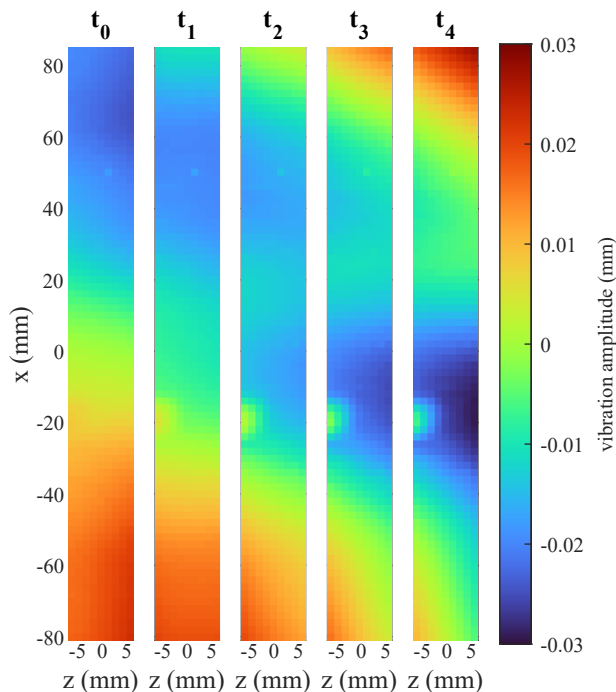
Fig. D.6. **Surface scan of TPU robot with 6 big LRA's**, spacing $\delta = 30mm$, and input signals with $f = 250\,Hz$, wavelength $\lambda = 240\ mm$ and $\varphi = \pi/4$. The amplitude in y-direction of the response to this signal is visualized over the full bottom surface of the robot, with the width in z-direction and length in x-direction. The four consecutive time steps are $2.5e - 4$ seconds apart.

existed of sending a set of signals with for each set a different fixed phase shift φ, which induced a metachronal wave along the robot. The wavelength of this wave, along with the average amplitude and TWR for positive and negative phase shifts can be found in the tables below.

In the tables can be found that the TWR is higher with frequency $f = 250\ Hz$ compared to $f = 350\ Hz$ for both forward traveling waves (negative phase shift) and backward traveling waves (positive phase shift). This may be due to the additional phase shift that exists with a frequency of $f = 350\ Hz$, visible in the phase plot in Figure D.3c.

TABLE D.5
RESULTS OF VIBROMETER SCANS WITH $f = 350\ Hz$

$\varphi\ (rad)$	$\lambda\ (mm)$	Positive		Negative	
		$A\ (\mu m)$	TWR	$A\ (\mu m)$	TWR
π	60	18.39	0.01	18.39	0.01
$2\pi/3$	90	17.36	0.05	22.04	0.20
$\pi/2$	120	16.50	0.12	19.69	0.23
$2\pi/5$	150	16.55	0.12	18.13	0.24
$\pi/3$	180	17.04	0.14	17.72	0.23
$2\pi/7$	210	17.42	0.12	17.64	0.22
$\pi/4$	240	17.60	0.13	17.66	0.21
$2\pi/9$	270	17.68	0.13	17.61	0.20
$\pi/5$	300	17.65	0.13	17.53	0.19
$\pi/6$	360	17.62	0.14	17.43	0.17
$\pi/9$	540	17.42	0.14	17.35	0.15

TABLE D.4
RESULTS OF VIBROMETER SCANS WITH $f = 250\ Hz$

$\varphi\ (rad)$	$\lambda\ (mm)$	Positive		Negative	
		$A\ (\mu m)$	TWR	$A\ (\mu m)$	TWR
π	60	15.85	0.02	15.86	0.02
$2\pi/3$	90	20.41	0.44	20.63	0.40
$\pi/2$	120	20.69	0.47	20.89	0.49
$2\pi/5$	150	20.48	0.43	20.63	0.49
$\pi/3$	180	20.46	0.41	20.49	0.50
$2\pi/7$	210	20.54	0.42	20.45	0.51
$\pi/4$	240	20.59	0.42	20.42	0.50
$2\pi/9$	270	20.65	0.42	20.42	0.49
$\pi/5$	300	20.69	0.43	20.42	0.48
$\pi/6$	360	20.72	0.44	20.40	0.48
$\pi/9$	540	20.70	0.45	20.40	0.46

APPENDIX E

PATHWAY DETECTION ALGORITHM

The pathways of the TPU robot are extracted from videos with the MATLAB algorithm described in this appendix. The videos are taken from above, see Figure E.7, from which the pathways of the 6 actuators can be detected to later extract the robot velocity.

The output of the code is a matfile with the same name as the video with a time vector tv, a 3 dimensional matrix $pathM$ with the x and y coordinates of the 6 actuators over time in meters, the pixel to meter ratio $p2m$, the flag variable that detects the missed actuators $DetectionMiss$ (which was 0 for all videos), and lastly input variable nA, which is the amount of actuators that needed to be detected. The detected pathways can be found in Appendix F.
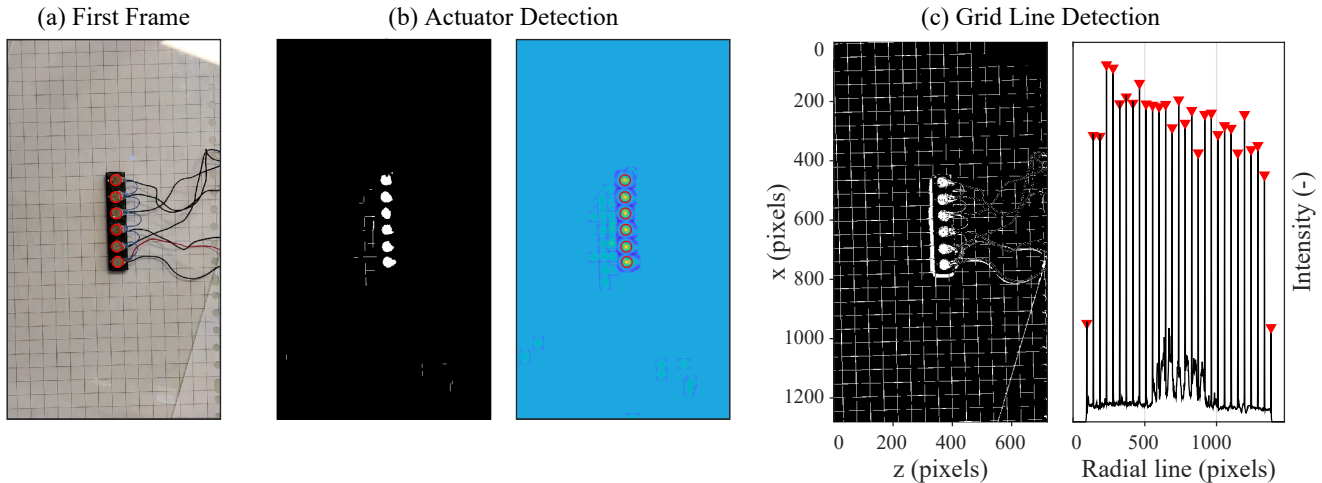
Fig. E.7. Visualization of different steps in the pathway detection algorithm. (a) Raw image of the first frame of one of the video's with the detected actuators surrounded by a red circle. (b) Process to detect actuators in the first frame. On the left the filtered and binarized frame is shown. On the right the 2D-cross correlation of this filtered and binarized image and a binary mask of an expected actuator is visualized using an HSV colormap. Here, yellow coloured areas correspond to peaks in the cross-correlation matrix. 6 peaks are marked as the center locations of the actuators. Both figures show the detected actuators with red circles around them. (c) Process to detect the grid lines in the first frame. On the left the filtered and binarized frame is shown. On the right the Radon transform with the highest intensity value for this filtered and binarized image is plotted. This Radon transform (91.5°) aligns with the grid lines, resulting in distinctive peaks which often correspond to the position of the grid lines on the radial line. The peaks that are derived to correspond to a grid line are marked with a red triangle. Here, a centimeter (the distance between 2 grid lines) was found to equal the width of 45.86 pixels on average.

First frame

In order to extract the pixel to meter conversion factor for each video, the code below takes the first frame of a video, converts this frame from RGB to grey scale, filters it and finally binarizes it to sufficiently isolate the grid lines in the background of the video. Then Radon transforms of this image are derived for the angles between 0° and 180°. Since the Radon transform contains a high intensity value when it aligns with a grid line, the peak finding function of MATLAB is used to find the expected locations of the grid lines. A variability check is then performed on the spacing between these expected grid lines, since the spacing between the real grid lines is equal, so the variability should be low. This way, the wrongly detected grid lines can be removed. The average pixel spacing between the remaining detected grid lines, which were spaced 1 cm apart, was finally multiplied by a factor 100 to obtain the pixel to meter conversion factor. The grid line detection process is partly visualized in Figure E.7c.

When the pixel to meter ratio is found, the locations of the 6 actuators in the first frame can be derived. For this derivation, the frame is first converted from a RGB to a HSV color map and subsequently filtered and then binarized in order to isolate the actuators of the robot. To further isolate the actuators, smaller remaining components in the binarized image are removed and the remaining components are closed with a circular structuring element object. Then a 2D-cross correlation is performed on the remaining image and an expected mask of an actuator, which is based on the pixel to meter conversion factor. A two dimensional peak searching algorithm from the MATLAB community file exchange called FastPeakFind is used to find the 6 highest peaks in the cross-correlation matrix which correspond to the center positions of the 6 actuators. Here too, a variability check on the actuator spacing is performed to verify if this spacing is consistent. The actuator detection process is partly visualized in Figure E.7b.

Remaining frames

For all the other frames, the search area is reduced to the area around the actuators from the previous frame to reduce the search time and avoid unwanted peaks around the edges. Then the actuators are detected in that frame following the same

detection algorithm as described before. However, to improve robustness the highest peak within a realistic travel distance (radius of an actuator) of each previously detected location is marked as the current actuator location, instead of marking the 6 highest peaks as the center position of the actuators.

MATLAB code

```matlab
clear all; clc; close all
%% Search names for videos
LoadDir = ''; % folder with files
Files = dir(LoadDir);
Files = {Files(~ismember({Files.name},{'.','..'})).name};
FilesI = 1:numel(Files);

SaveDir = '';
Exist = dir(SaveDir);
FilesI = find(cellfun(@(y) ~any(cellfun(@(x) strcmp(x,y),{Exist.name})),strrep(Files,
    'mp4','mat')));

% Loop for videos
for i = 1:FilesI
    disp(i) % Load video
    v = VideoReader([LoadDir Files{i}]);

    %% Starting flags and variables
    DetectionMiss = 0;
    Track = 0;
    nA = 6; % number of actuators

    tv = (0:v.NumFrames-1)'/v.FrameRate; % time vector for video

    path = zeros(v.NumFrames,6,2);

    % Loop for all frames
    for j = 1%:size(path,1)

        % Read frame j
        frame = read(v,j);

        % For first frame
        if j==1

            % Crop frame to relevant area
            switch i
                case {6,7}
                    X = 365:920;
                    Y = 195:520;
                case num2cell(10:16)
                    X = 280:570;
                    Y = 430:900;
                otherwise
                    X = 1:size(frame,2);
                    Y = 1:size(frame,1);
            end

            % Filter grid to extract pixel to mm ratio
            tmp = rgb2gray(frame(Y,X,:));
            tmp(tmp<60 | tmp > 140) = 255;
            tmp = imbinarize(imcomplement(tmp));
```

```matlab
        figure(i*3-1)
        subplot 121
        imshow(tmp);
        axis('on', 'image');
        title('Processed Image')

        % Do radon transform and get maximal projection
        Theta = 0:0.1:180;
        r = radon(tmp,Theta);
        M = max(r(:));
        [~,J] = find(r == M);
        [~,J] = min(abs(Theta-(Theta(J)+90)));
        rM = r(:,J);
        subplot 122
        plot(rM,'b-','LineWidth',2);
        title(['Maximum radon transform intensity for ' num2str(Theta(J)) char ...
            (176)])
        xlabel('Pixel width')
        ylabel('Intensity')
        grid on
        hold on

        % Find peaks
        [vPeaks,PeaksI] = findpeaks(rM,'MinPeakProminence',M*0.1);

        % Get the spacing between the peaks
        Spacing = diff(PeaksI);
        while std(Spacing) > 1
            I2 = find(Spacing < 0.9*median(Spacing));
            I2 = (1:numel(Spacing)+1~=I2(2:2:end));
            PeaksI = PeaksI(I2);
            vPeaks = vPeaks(I2);
            disp('High varialibity in detected grid lines spacing. Removed ...
                inconsistent grid line detections.')
            Spacing = diff(PeaksI);
        end
        plot(PeaksI,vPeaks, 'r+', 'LineWidth', 2, 'markerSize', 17);

        % Get the mean grid spacing.
        p2cm = mean(Spacing); % Pixels/cm
        sgtitle(sprintf('Analysed scale of image = %.1f Pixels/cm.',p2cm));

        % Make circle mask
        r = round(0.8*p2cm/2);
        tmp = -r:r;
        XX = meshgrid(tmp,tmp);
        maskA = zeros(size(XX));
        maskA((XX.^2+XX'.^2)<=r^2)=1;

        % Make margin for cropping subsequent frames
        marg = r;
        margA = (r+marg)*[-1,1];
    % For all other frames
    else
        % Reduce search area to neighbourhood of last detection
        X = feval(@(x) [min(x),max(x)]+margA,p(:,1));
        Y = feval(@(x) [min(x),max(x)]+margA,p(:,2));
        X = X(1):X(2);
```

```matlab
        Y = Y(1):Y(2);
    end

    % Filter actuators
    frame = frame(Y,X,:);
    tmp = rgb2hsv(frame);
    mask = feval(@(x,y) x > y(1) & x < y(2),tmp(:,:,1),[0.07 0.15]) &...
        feval(@(x,y) x > y,tmp(:,:,2),0.2)&...
        feval(@(x,y) x > y(1) & x < y(2),tmp(:,:,3),[0.2 0.7]);
    mask = bwareaopen(mask,10);
    SE = strel('disk',3);
    mask = imclose(mask,SE);

    % Detect actuators
    C = normxcorr2(maskA,mask);
    C = C(r+1:end-r,r+1:end-r);

    [tmp2,I] = FastPeakFind(C);
    [~,I] = sort(C(logical(I)),'descend');
    tmp2 = reshape(tmp2,2,[])';
    tmp2 = tmp2+[X(1),Y(1)]-1;

    % Order actuators from 1 to 6
    tmp2 = tmp2(I,:);
    if j>1
        for k = 1:6
            if all(pdist2(tmp2,pOld(k,:))>=marg)
                p(k,:) = pOld(k,:);
                DetectionMiss = DetectionMiss+1;
            else
                p(k,:) = tmp2(find(pdist2(tmp2,pOld(k,:))<marg,1),:);
            end
        end
    else
        [~,I] = sort(vecnorm(tmp2(1:nA,:)'));
        p = tmp2(I,:);
    end

    pOld = p;
    path(j,:,:) = p;

    % Plot
    if j==1
        f = figure(i*3);
%         f.WindowState = 'Maximized';
        nPlots = 4;
        for k = 1:nPlots
            subplot(1,nPlots,k)
            switch k
                case 1
                    imshow(frame)
                case 2
                    imshow(tmp)
                case 3
                    imshow(mask)
                case 4
                    imagesc(C)
            end
```

```matlab
                axis('on', 'image');
                sgtitle(['Frame ' num2str(j)])

                arrayfun(@(x) viscircles(x,p-[X(1),Y(1)]+1,repmat(r,length(p),1),'
                    EdgeColor','r','LineWidth',2),f.Children(2:end));
                drawnow
            end
%                   subplot(1,nPlots,2)
%                   impixel
%                   return
            figure(1)
        end

        % Check if the space between detected actuators is consistent
        if Track || norm(std([diff(p(:,1)),diff(p(:,2))]))>5
            imshow(frame)
            axis('on', 'image');
            viscircles(p-[X(1),Y(1)]+1,repmat(r,length(p),1),'EdgeColor','r','
                LineWidth',2);
            title(num2str(i))
            drawnow
            if std(vecnorm([diff(p(:,1)),diff(p(:,2))]'))>10
                return
            end
        end
    end
    if j==1
        continue
    end

    %%
    p2m = p2cm*100;
    pathM = path/p2m;
    pathM(:,:,2) = size(read(v,j),1)/p2m-pathM(:,:,2);

    %% Visualize extracted pathways
    disp(DetectionMiss)
    figure(i*3+1)

    plot(pathM(:,:,1),pathM(:,:,2))
    lgd = legend(append('Actuator',string(1:nA)));
    legend('boxoff')
    lgd.AutoUpdate = 'off';

    hold on
    plot(pathM(1,:,1),pathM(1,:,2),'k.','MarkerSize',30)
    xlabel('x (m)')
    ylabel('y (m)')

    axis equal

    %% Save pathways
    save([SaveDir erase(Files{i},'.mp4')],'tv','pathM','p2m','DetectionMiss','nA')
end
```

APPENDIX F

RAW DATA FROM PATHWAY DETECTION OF VELOCITY EXPERIMENTS

In this appendix the detected pathways of the 6 actuators are visualized for each video. The magnitude of the average robot velocity over time is also shown for forward and backward motion.
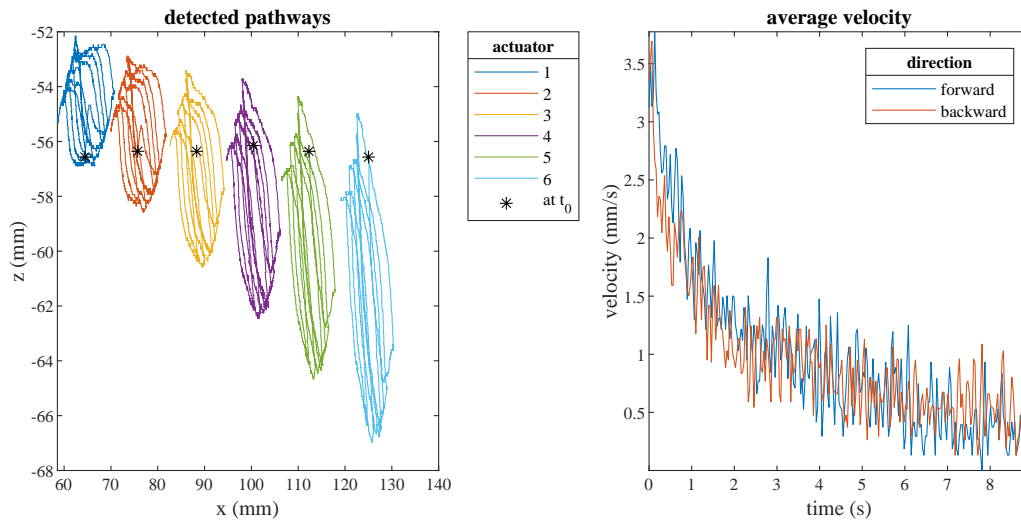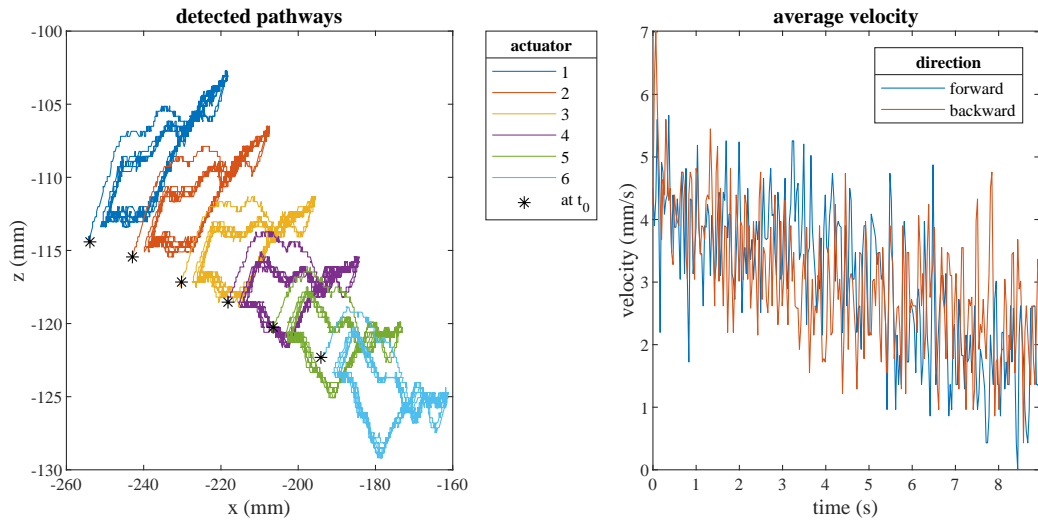

Fig. F.8. **Robot pathway and velocity for metachronal wave with frequency** $f = 235 \ Hz$**, wavelength** $\lambda = 36 \ mm$ **and input phase shift** $\varphi = 2\pi/3$**.**
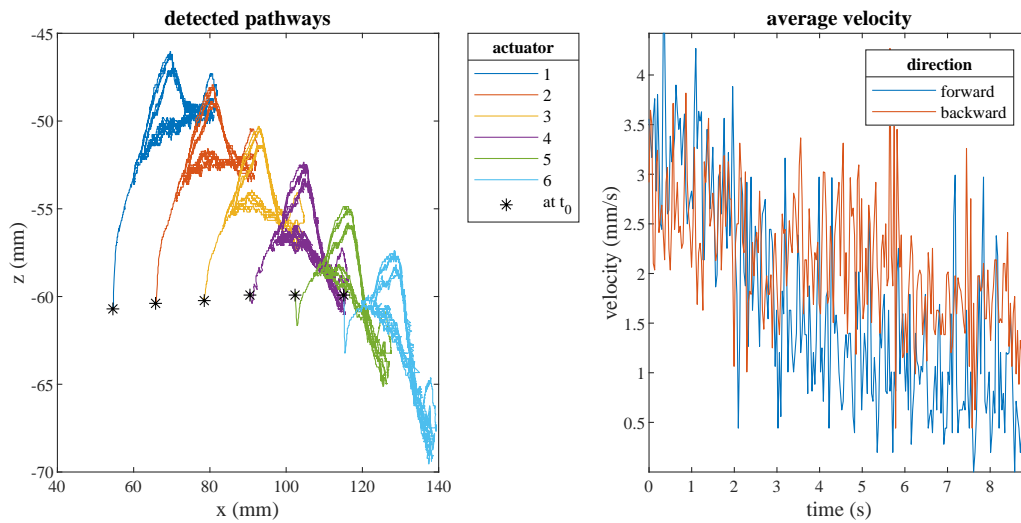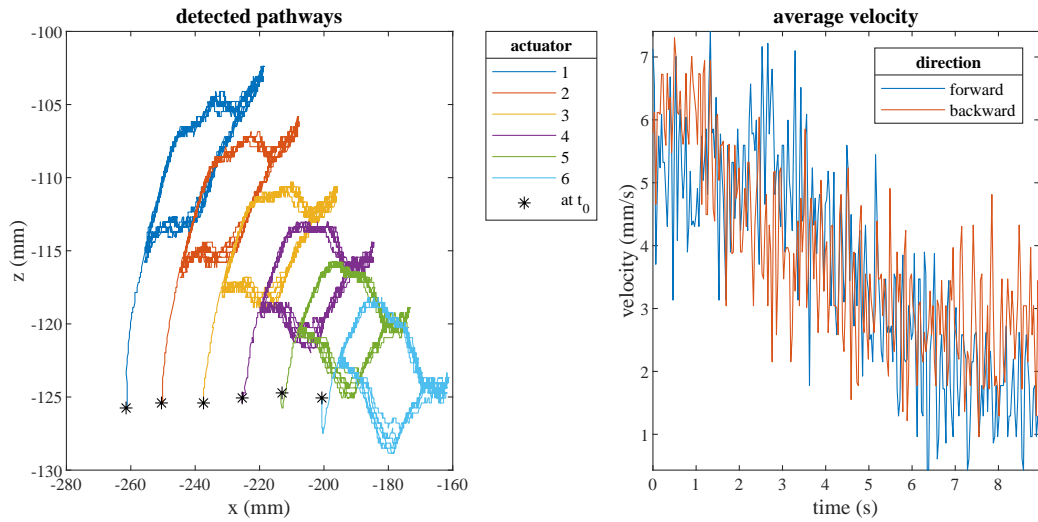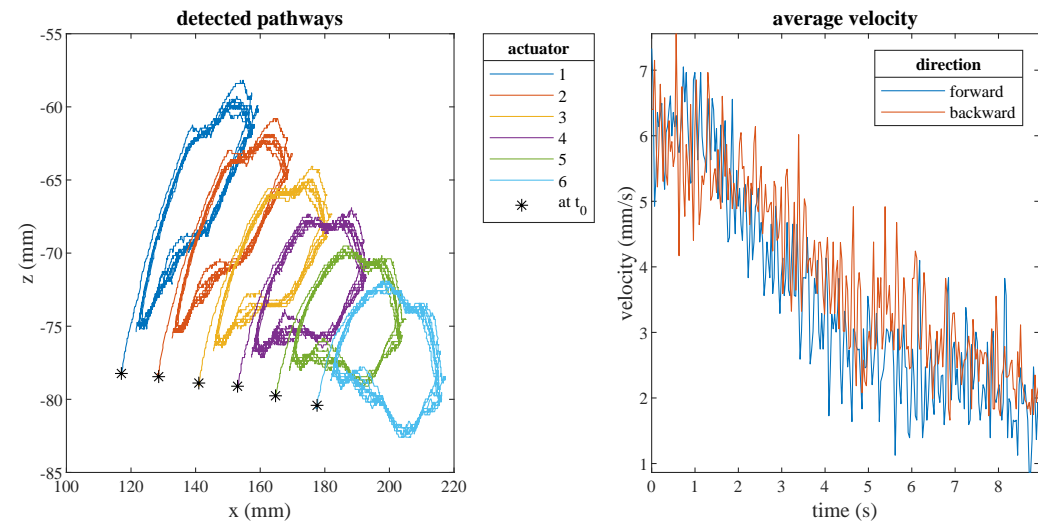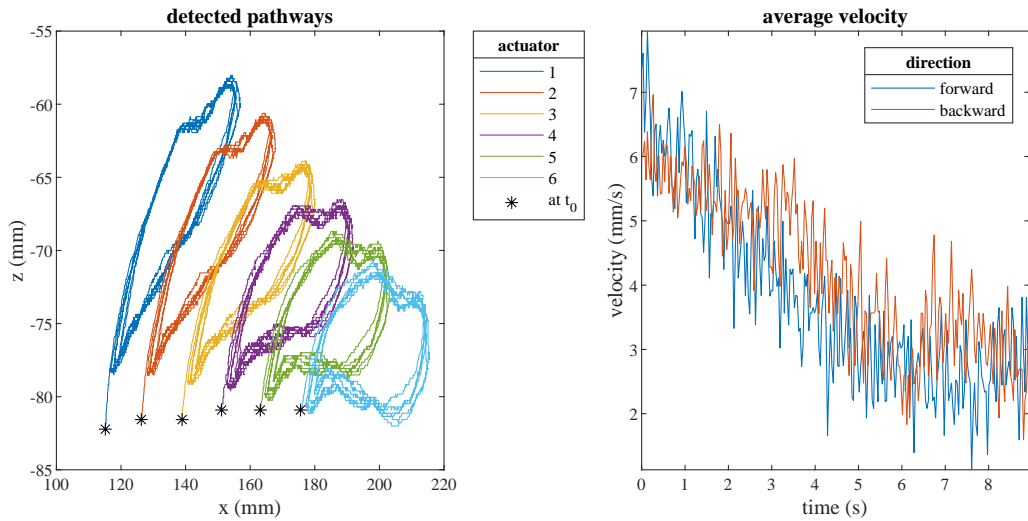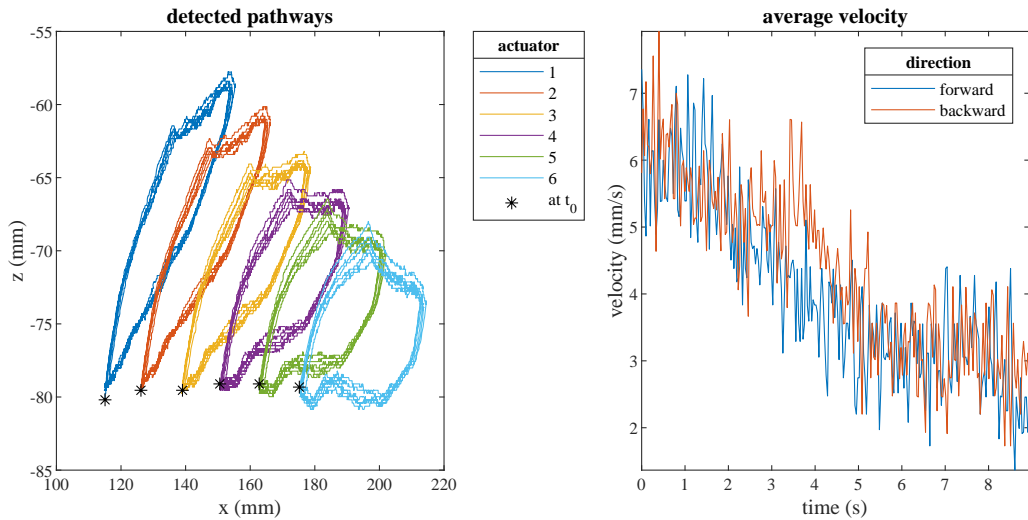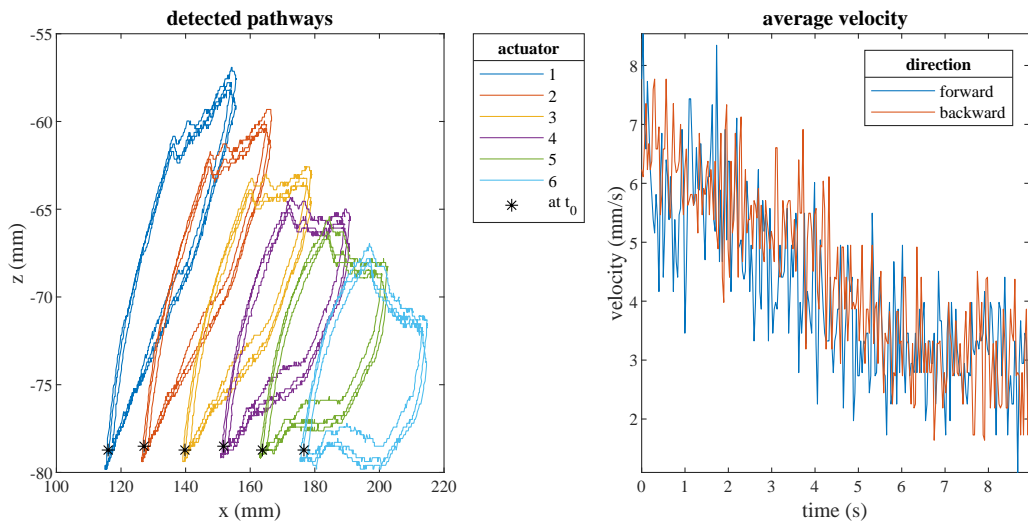

Fig. F.9. **Robot pathway and velocity for metachronal wave with frequency** $f = 235 \ Hz$**, wavelength** $\lambda = 48 \ mm$ **and input phase shift** $\varphi = \pi/2$**.**

Fig. F.10. **Robot pathway and velocity for metachronal wave with frequency** $f = 235\ Hz$**, wavelength** $\lambda = 60\ mm$ **and input phase shift** $\varphi = 2\pi/5$**.**
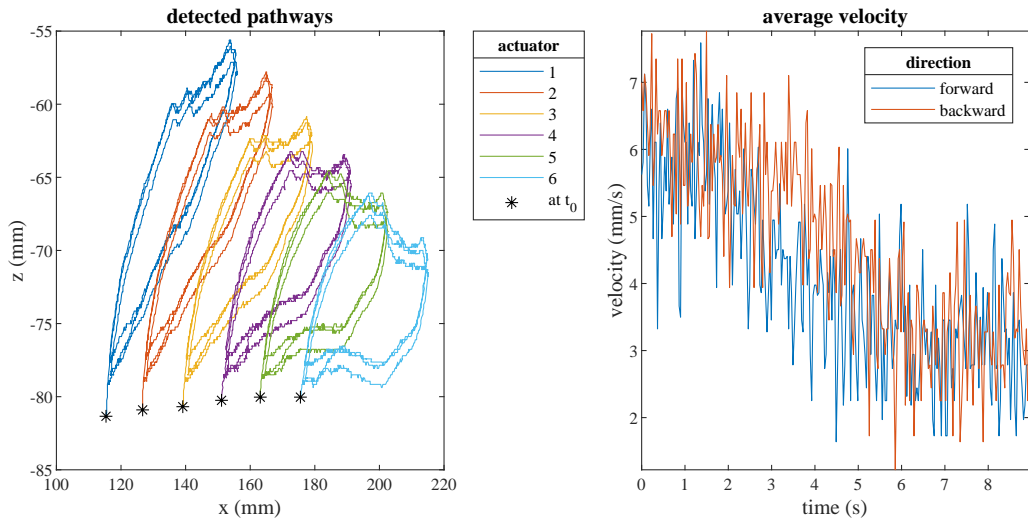

Fig. F.11. **Robot pathway and velocity for metachronal wave with frequency** $f = 235\ Hz$**, wavelength** $\lambda = 72\ mm$ **and input phase shift** $\varphi = \pi/3$**.**

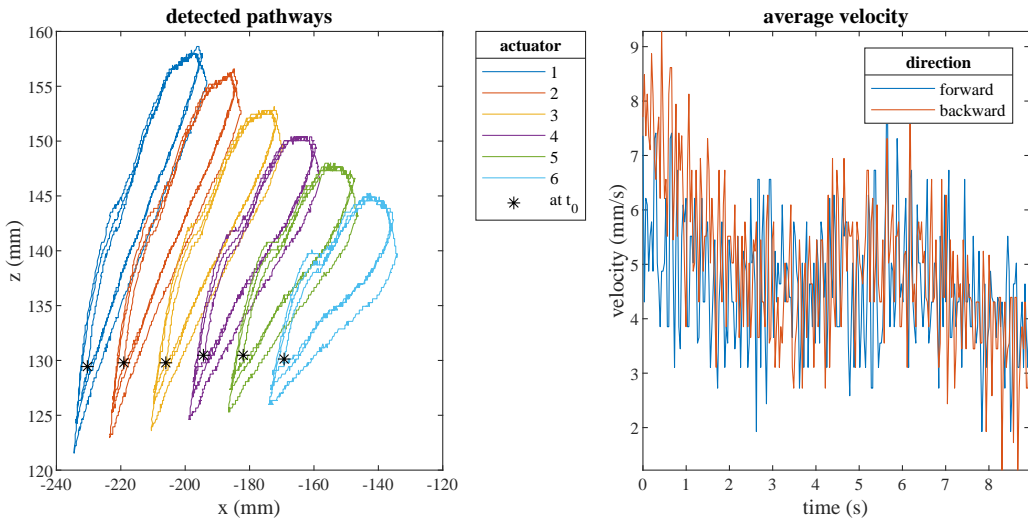

Fig. F.12. **Robot pathway and velocity for metachronal wave with frequency** $f = 235\ Hz$**, wavelength** $\lambda = 84\ mm$ **and input phase shift** $\varphi = 2\pi/7$**.**

Fig. F.13. Robot pathway and velocity for metachronal wave with frequency $f = 235\ Hz$, wavelength $\lambda = 96\ mm$ and input phase shift $\varphi = \pi/4$.

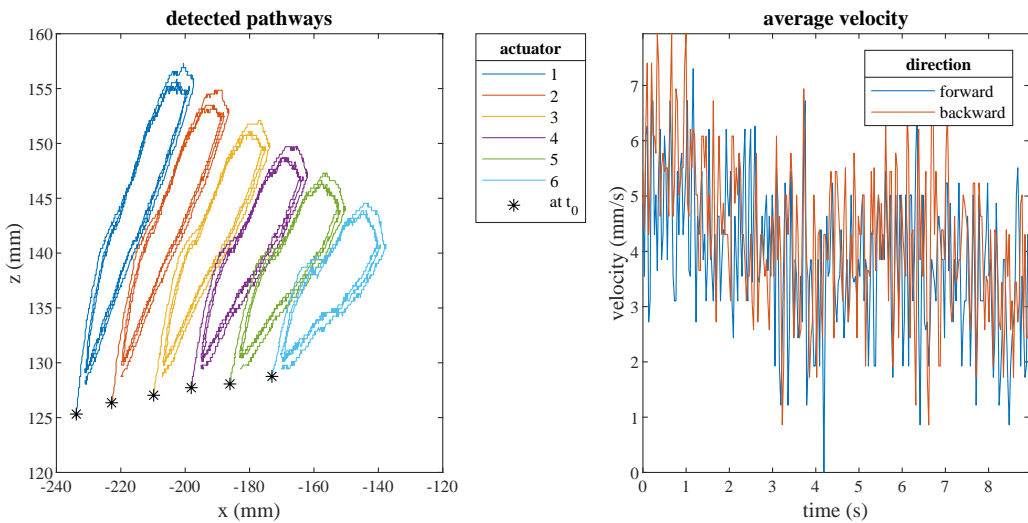**Fig. F.14. Robot pathway and velocity for metachronal wave with frequency $f = 235\ Hz$, wavelength $\lambda = 108\ mm$ and input phase shift $\varphi = 2\pi/9$.**

Fig. F.15. Robot pathway and velocity for metachronal wave with frequency $f = 235\ Hz$, wavelength $\lambda = 120\ mm$ and input phase shift $\varphi = \pi/5$.
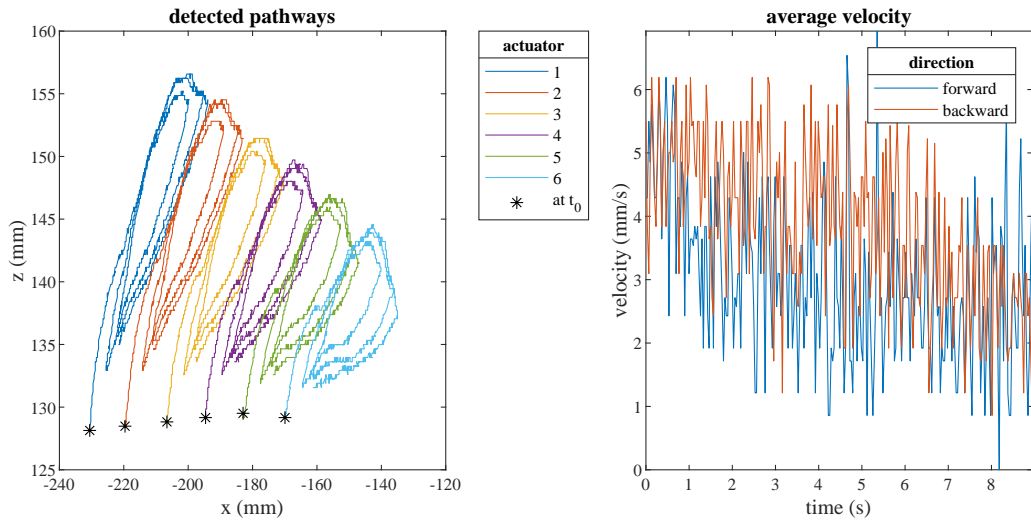
Fig. F.16. **Robot pathway and velocity for metachronal wave with frequency** $f = 235\ Hz$**, wavelength** $\lambda = 120\ mm$ **and input phase shift** $\varphi = \pi/5$**.**
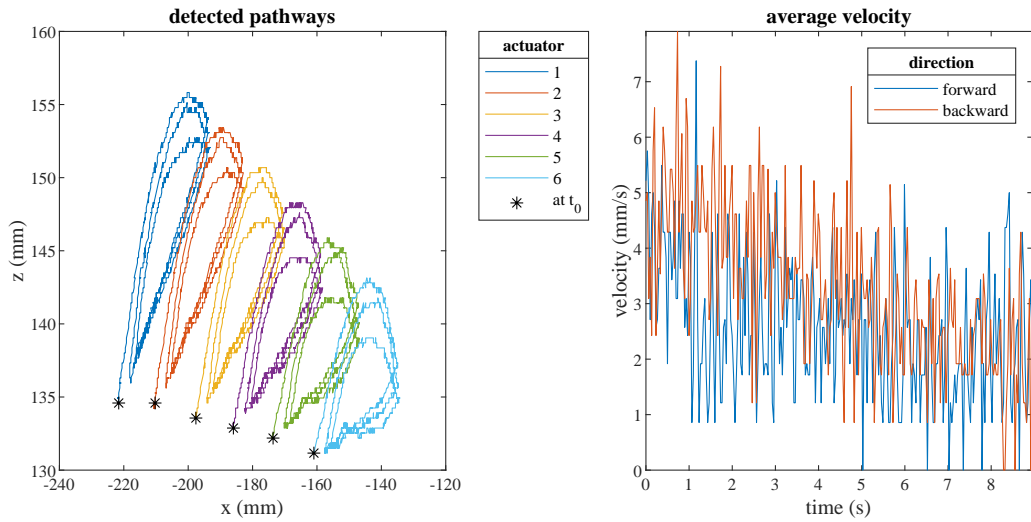

Fig. F.17. **Robot pathway and velocity for metachronal wave with frequency** $f = 235\ Hz$**, wavelength** $\lambda = 144\ mm$ **and input phase shift** $\varphi = \pi/6$**.**

Fig. F.18. **Robot pathway and velocity for metachronal wave with frequency** $f = 235\ Hz$**, wavelength** $\lambda = 168\ mm$ **and input phase shift** $\varphi = \pi/7$**.**

Fig. F.19. **Robot pathway and velocity for metachronal wave with frequency** $f = 235\ Hz$**, wavelength** $\lambda = 192\ mm$ **and input phase shift** $\varphi = \pi/8$**.**

Fig. F.20. **Robot pathway and velocity for metachronal wave with frequency** $f = 235\ Hz$**, wavelength** $\lambda = 216\ mm$ **and input phase shift** $\varphi = \pi/9$**.**
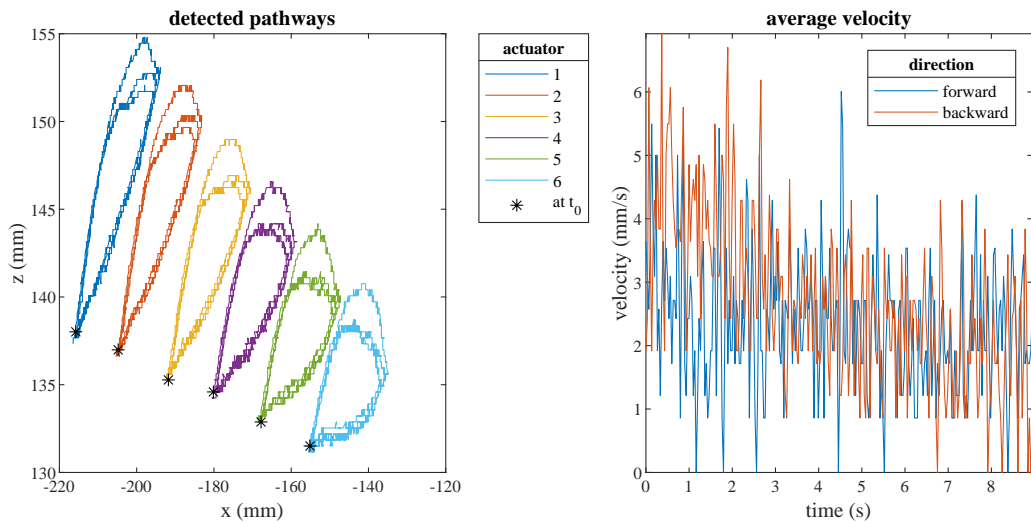

Fig. F.21. **Robot pathway and velocity for metachronal wave with frequency** $f = 235\ Hz$**, wavelength** $\lambda = 240\ mm$ **and input phase shift** $\varphi = \pi/10$**.**
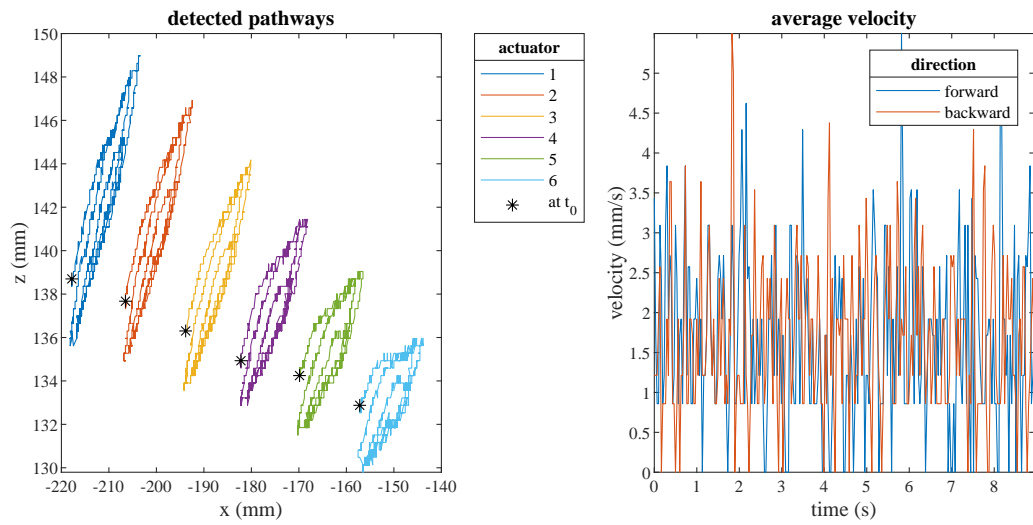
detected pathways

average velocity

Fig. F.22. **Robot pathway and velocity for metachronal wave with frequency** $f = 235\ Hz$**, wavelength** $\lambda = 377\ mm$ **and input phase shift** $\varphi = 0.2$**.**
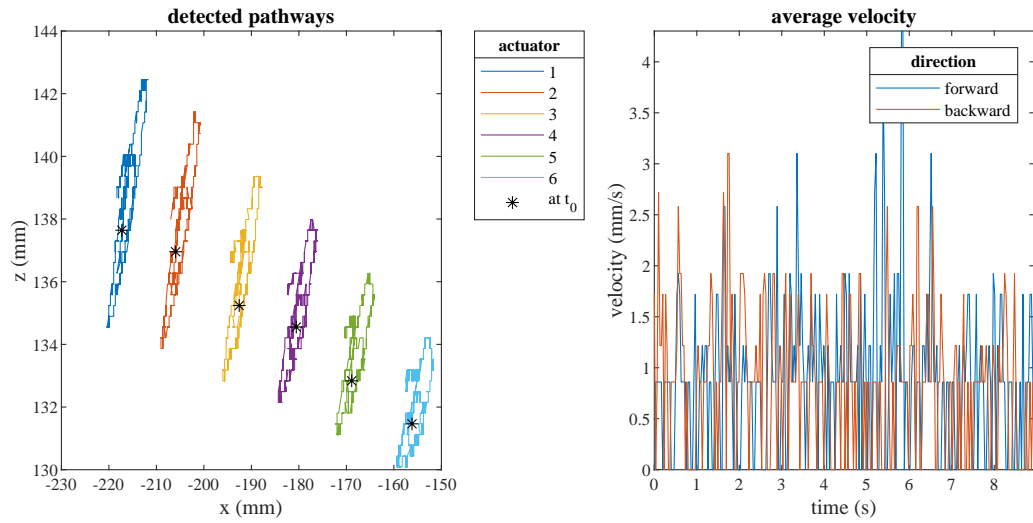
detected pathways

average velocity

Fig. F.23. **Robot pathway and velocity for metachronal wave with frequency** $f = 235\ Hz$**, wavelength** $\lambda = 754\ mm$ **and input phase shift** $\varphi = 0.1$**.**